

## Severe Thunderstorm Observation and Modeling – A Review

Someshwar Das

Department of Atmospheric Science, Central University of Rajasthan  
Email: somesh@curaj.ac.in, somesh03@gmail.com

### ABSTRACT

*One of the nature's most spectacular phenomenon; the thunderstorm is reviewed from the point of their formation, intensity, modeling, forecasting and field research. The thunderstorms are reviewed in particular with regard to their characteristics over the Indian sub-continent. There is a need for more concerted efforts on conducting field experiments, with convective scale data assimilation and ensemble modeling to improve the skills of forecasting the thunderstorms.*

**Keywords:** Mesoscale, assimilation, ensemble modeling and parameterization

### 1. Introduction

Thunderstorms occur almost everywhere on the earth's surface. It is estimated that at any given time there are about 2000 thunderstorms taking place on the globe (<http://www.nssl.noaa.gov/education/svrwx101/thunderstorms/>). While they occur both during the summer and the winter seasons, their frequency is highest during the pre-monsoon season over the Indian subcontinent. Three ingredients that must be present for a thunderstorm to occur are moisture, instability, and lifting. Therefore they also occur during the winter season associated with the Western Disturbances even though the land is cool. Additionally, there is a fourth ingredient (wind shear) for severe thunderstorms. Instability is what allows air in the low levels of the atmosphere to rise into the upper levels of the atmosphere. The instability supports the atmosphere for deep convection and thunderstorms. Instability can be increased through daytime heating. Lifting gives a parcel of air the impetus to rise from the low levels of the atmosphere to the elevation where positive buoyancy is realized. Very often, instability will exist in the middle and upper levels of the troposphere but not in the lower troposphere.

It is lift that allows air in the low levels of the troposphere to overcome low level convective inhibition. Lift is often referred to as a trigger mechanism. There are many lift mechanisms, some of them are fronts, low level convergence, low level warm air advection (WAA), low level moisture advection, mesoscale convergence boundaries such as

outflow and sea breeze boundaries, orographic upslope, frictional convergence, vorticity, and jet streak. All these processes force the air to rise. The region that has the greatest combination of these lift mechanisms is often the location that storms first develop. Moisture and instability must also be considered. A thunderstorm will form first and develop toward the region that has the best combination of: high PBL moisture, low convective inhibition, CAPE and lifting mechanisms. Thunderstorms often form in clusters with numerous cells in various stages of their life cycle. While each individual cell behaves as a single cell, the prevailing conditions are such that as the first cell matures, it is carried downstream by the upper level winds and new cell forms upwind of the previous cell. Figure 1 illustrates a multi cell cluster.

### 2. Why are Thunderstorms Furious?

The ferocity of thunderstorm depends on its damage potential in terms of the strength of wind, ability for a lightning strike, size of hail stones, and flash floods. For a severe thunderstorm, the ingredients that must be present are moisture, instability, lift and strong speed and directional storm relative wind shear. Wind shear aids in the following: Tilting a storm (displacing updraft from downdraft), allows the updraft to sustain itself for a longer period of time, allows the development of a mesocyclone, and allows rotating air to be ingested into the updraft (tornadogenesis). Severe storms also tend to have these characteristics over ordinary

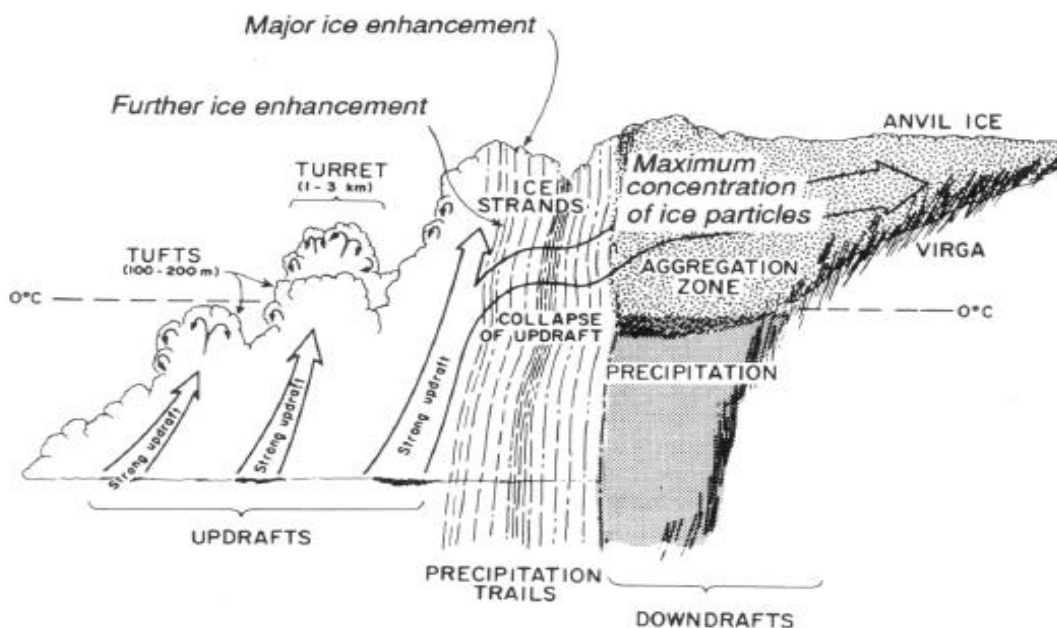


**Figure 1: Illustration of a Typical Multi Cell Storm. Upper Panel from National Weather Service (NOAA), and Lower Panel from Houze (1993).**

thunderstorms: higher CAPE, drier air in the middle levels of the atmosphere (convective instability), better moisture convergence, Baroclinic atmosphere, and more powerful lift.

**2.1 Mechanism of Gale wind**

Wind is stronger when the pressure gradient is high. Strong winds experienced during a thunderstorm are due to the downdrafts beneath the cumulonimbus. Rain from the storm evaporates below the cloud, causing the air to cool beneath it. This cold air is heavy and crashes into the ground below. When it hits the ground, this cold air must turn sideways, and the result is strong winds. These winds are known as microbursts. Wind speeds in microbursts can exceed 160 km h<sup>-1</sup> and cause significant damage even though they only last for 5 to 15 minutes. A typical thunderstorm is made up of a single cumulonimbus (CB) cloud. The CB cloud consists of strong vertical updrafts and downdrafts. Depending upon their intensity (wind speed), they are classified as Gust wind, Squall wind, Light Nor’wester, Moderate Nor’wester, Severe Nor’wester, or a Tornado (Table 1).

In a typical cyclone, the central pressure can drop to about 900 hPa and the average radius of maximum wind (RMW) is estimated about 47 km (Hsu and Yana, 1998). In case of a tornado, the RMW is typically about 46-150 m with an extreme case of about 800 m (USDE, 2009 and Wurman et al., 2007). The highest peak sustained wind for 1 minute is recorded

Wind Speed Km/hr	Types
30-40	Gust Wind
41-60	Squally Wind
61-90	Light Nor’wester
91-120	Moderate Nor’wester
121-149	Severe Nor’wester
>150	Tornado

as 345 km h<sup>-1</sup> and 260 km h<sup>-1</sup> for 10 minutes (JMA, 2017 and NHC, 2016). Extreme wind speed recorded in a tornado is about 484 ± 32 km/h (F5), the central pressure is estimated about 810 hPa with a pressure drop of 100 hPa (CSWR, 2006; Walter, 1997).

## 2.2 Mechanism of Lightning and Thunder

Lightning is caused by an electrical discharge of electrons moving very quickly from one place to another. These electrons move so quickly that they superheat the air around them causing it to glow. Thunderstorms are created

the cloud and gravity pulls the larger water or ice particles towards the bottom of the cloud. This separation of smaller positively charged particles and the larger negatively charged particles create an electrical imbalance with an enormous electric potential of millions of volts across the storm cloud. The laws of physics

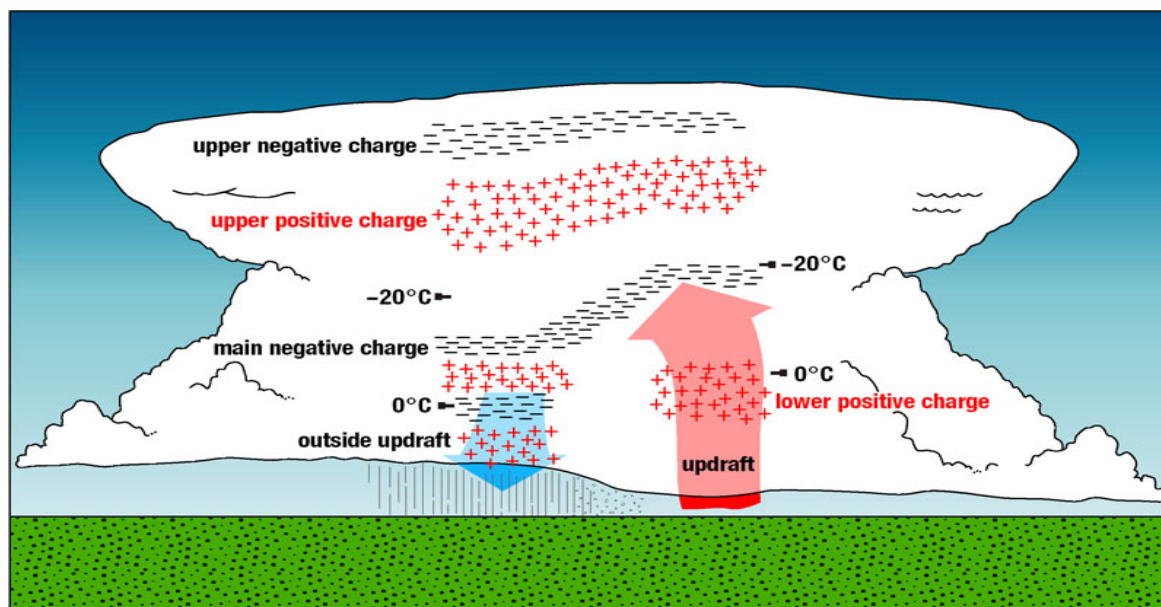


**Figure 2: Schematic of the Basic Charge Structure in the Convective Region of a Thunderstorm (source: <http://www.nssl.noaa.gov/education/svrwx101/lightning/types/>).**

by strong rising air currents called updrafts forming Cumulonimbus clouds. These updrafts create winds of about 80 km h<sup>-1</sup> (or more) rising several miles into the air to form Cumulonimbus clouds. Warm updrafts and cooler weaker downdrafts create turbulence within thunderclouds resulting in the interaction of tiny water particles and microscopic ice crystals called hydrometeors. The continuous collisions of the water and ice create large and small particles. The different movement characteristics of these varying sized particles in turn create electrical charges within the cloud. Fig. 2 illustrates the distribution of charges in a typical thunderstorm.

It is believed that smaller particles (less than 100 micrometers) acquire a positive charge, while larger particles gain a negative charge. Movement of air inside the cloud combined with the effects of gravity causes these differently sized water particles to separate. Updrafts carry the tiny particles to the top of

requires this electrical difference to be neutralized. Lightning is formed as tremendous currents travel across the air to correct the huge imbalance of negative electrons created within the storm cloud. More detailed information on lightning can be found in <http://www.aharfield.co.uk/lightning-protection-services/how-lightning-is-formed>.

The bright glow from lightning is caused by the immense currents (about 200,000 amps) super heating the air it is traveling along to 3 ½ times hotter than the surface of the sun to the order of 20,000 degrees C. The sound of thunder is caused by the same superheated air expanding rapidly and creating a supersonic shock wave, which then decays to an acoustic wave as it propagates away from the lightning channel. As a lightning strike is not one continuous bolt of lightning, but a series of lightning bursts traveling along stepped leaders (typically 30m in length) the sound created is not one single report or boom, but a series of them. On the return stroke, each

stepped leader is discharged from the bottom up super heating air and creating a shock wave at different altitudes. These differently timed shock waves at different altitudes give the rumble effect during a lightning strike. A series of secondary strokes can also travel along the same ionised channel as the initial return stroke making the thunderclap oscillate in volume as secondary shock waves are generated.

Lightning is a sure sign of the presence of thunderstorm. Observations indicate that the number of lightning strikes over the earth per second is about 100 of which 80% are in-cloud flashes and 20% are cloud-to-ground flashes. This implies that there are about 8,640,000 lightning strikes over the earth per day. Each year, lightning flashes about 1.4 billion times over Earth. The greatest flash density averages only 36 discharges per square kilometer per year. A lightning flash is composed of a series of strokes with an average of about four. The length and duration of each lightning stroke vary, but typically average about 30 microseconds. An average bolt of lightning carries a current of 30 kilo amperes, transfers a charge of 5 coulombs, has a potential difference of about 100 megavolts and dissipates 500 mega joules (enough to light a 100 watt light bulb for 2 months).

Each year lightning strikes kill many people and animals. Lightning causes thousands of fires and billions of Rupees in damage to buildings, communication systems, power lines and electrical systems. Lightning also costs airlines billions of Rupees in flight rerouting and delays. The Lightning Imaging Sensor (LIS) aboard TRMM measures total lightning (intracloud and cloud-to-ground) using an optical staring imager. This sensor identifies lightning activity by detecting changes in the brightness of clouds as they are illuminated by lightning electrical discharges (Christian et al. 1999). Albrecht et al. (2009) constructed climatology maps for the tropical region based on 10 years (1998-2007) of LIS total lightning data. His study showed that more lightning occurs over land than ocean and more lightning occurs near the equator than near the poles. The highest mean flash rate on the earth is 17.43 flash km<sup>-2</sup> year<sup>-1</sup>, and is located over the Maracaibo Lake in Venezuela (9.6250N, 71.8750W). The

maximum flash rate during March-April-May (MAM) is located at Sunamganj, Bangladesh, at the foot of Khasi Hills, Meghalaya, India, before the onset of Indian Monsoon (Albrecht et al., 2009; Das et al., 2010).

### 3. How Can We Model Thunderstorms?

A basic characteristic of the convective cloud models is that their governing equations are non-hydrostatic since the vertical and horizontal scales of convection are similar. Presently, mesoscale models having horizontal resolution  $\leq 10$  km are also used for simulation and prediction of regional weather systems. These models can be used for a wide variety of applications including simulation and prediction of severe storms and tropical cyclones. In order to adequately model the thunderstorms, the fundamental physical and mathematical laws governing the dynamics and thermodynamics of the clouds need to be implemented in a form which is physically meaningful, mathematically rigorous, and computationally efficient. Numerous physical factors linked to the dynamical and thermodynamical characteristics of the clouds need to be addressed.

The modeling of storms depends on the requirement. The storm models may be one, two or three dimensional. Single Column Models (SCMs) or one dimensional models are used for investigating individual physical processes in idealized condition. The SCMs can be considered as a single grid box of a climate model in which field observations may be used to test the parameterization of a physical process. Since the SCMs do not interact with the neighboring grid columns, the effects of the surrounding grid boxes are specified in terms of the large-scale advective forcings to run the SCMs (Xu and Randall, 1996, Das et al., 1987, 1998, 1999, Liu et al., 2001). The one-dimensional are generally axi-symmetric in which cumulus cloud is assumed to be a function of  $t$ ,  $r$ ,  $\psi$ , and  $z$ , where  $t$  is time;  $r$  is radius;  $\psi$  is tangential angle; and  $z$  is height (Yanai et al., 1973; Arakawa and Schubert, 1974; Anthes, 1990; Nitta, 1975; Johnson, 1993; Fritsch and Chappell, 1980; Houze et al., 1990). Two-dimensional (2D) anelastic cloud model was developed to study cloud development under the influence of the surrounding environment

(Ogura and Phillips 1962). After Global Atmospheric Research program's Atlantic Tropical Experiment (GATE, 1974), cloud ensemble modeling was developed to study the collective feedback of clouds on the large-scale tropical environment with the aim of improving cumulus parameterization in large-scale models (i.e., Soong and Tao 1980; Tao and Soong 1986; Tao et al. 1987; and many others), a quest that continues to this day.

Considerable progress has also been made in microphysical parameterizations in three-dimensional cloud models. Lin et al. (1983) developed a three-class ice scheme that includes many microphysical processes. Cotton et al. (1986) extended their two-class ice scheme to three classes. To evaluate the performance of several ice parameterizations, McCumber et al. (1991) simulated tropical squall-type and nonsquall-type convections using a three-dimensional cloud model. The

$$\frac{\partial}{\partial x}(\rho_0 u) + \frac{\partial}{\partial y}(\rho_0 v) + \frac{\partial}{\partial z}(\rho_0 w) = 0, \quad (1)$$

$$\frac{du}{dt} - fv = -\frac{\partial}{\partial x}(c_p \theta_{v0} \pi') - \frac{\partial}{\partial x}(\overline{u''u''}) - \frac{\partial}{\partial y}(\overline{u''v''}) - \frac{1}{\rho_0} \frac{\partial}{\partial z}(\rho_0 \overline{u''w''}), \quad (2)$$

$$\frac{dv}{dt} + fu = -\frac{\partial}{\partial y}(c_p \theta_{v0} \pi') - \frac{\partial}{\partial x}(\overline{u''v''}) - \frac{\partial}{\partial y}(\overline{v''v''}) - \frac{1}{\rho_0} \frac{\partial}{\partial z}(\rho_0 \overline{v''w''}), \quad (3)$$

$$\begin{aligned} \frac{dw}{dt} = & -\frac{\partial}{\partial z}(c_p \theta_{v0} \pi') + g \left( \frac{\theta'}{\theta_0} + 0.61q_v - q_c - q_i - q_r - q_s - q_g \right) \\ & - \frac{\partial}{\partial x}(\overline{u''w''}) - \frac{\partial}{\partial y}(\overline{v''w''}) - \frac{1}{\rho_0} \frac{\partial}{\partial z}(\rho_0 \overline{w''w''}), \end{aligned} \quad (4)$$

In the process of cloud modeling during the last decades, it was clearly realized that one- and two-dimensional cloud models are usually not capable of realistically simulating the complex behavior of convective systems. With the help of increasingly powerful computers, three-dimensional models have been used to simulate the development of an ensemble of cumulus clouds with random heating (Tao and Soong, 1986). Donner et al. (1999) simulated deep convection and its associated mesoscale circulations observed during the GATE.

three-dimensional cloud models can be classified into two types: one is based on the anelastic system of equations and the other on the fully compressible system of equations. Whether they are anelastic or fully compressible, practically all of the three dimensional cloud models developed so far view the dynamics of convection mainly in terms of the pressure gradient and buoyancy forces in the context of the momentum equation. Here we present a three-dimensional anelastic cloud model based on the vorticity

$$c_p \pi_0 \frac{d\theta}{dt} + L \frac{dq_v}{dt} = -\frac{1}{\rho_0} \left[ \frac{\partial}{\partial x}(\rho_0 \overline{u''h''}) + \frac{\partial}{\partial y}(\rho_0 \overline{v''h''}) + \frac{\partial}{\partial z}(\rho_0 \overline{w''h''}) \right] + Q_R + Q_A, \quad (5)$$

$$\begin{aligned} \frac{dq_x}{dt} = & \frac{1}{\rho_0} \left[ \frac{\partial}{\partial z}(\rho_0 V_x q_x) \right] - \frac{1}{\rho_0} \left[ \frac{\partial}{\partial x}(\rho_0 \overline{u''q''_x}) + \frac{\partial}{\partial y}(\rho_0 \overline{v''q''_x}) + \frac{\partial}{\partial z}(\rho_0 \overline{w''q''_x}) \right] \\ & + P_x + C_x + Q_{A,x}, \end{aligned} \quad (6)$$

equation based on Jung and Arakawa (2007, 2008).

Where  $u$ ,  $v$ , and  $w$  are the  $x$ -,  $y$ -, and  $z$ -components of velocity, respectively,  $\rho$  the density,  $f$  the Coriolis parameter,  $g$  the gravitational acceleration,  $\theta$  the potential temperature,  $\theta_v$  the virtual potential temperature defined by  $\theta_v \equiv \theta (1 + 0.61q_v)$ ,  $q$  the mixing ratio of water vapor ( $v$ ), cloud water ( $c$ ), cloud ice ( $i$ ), rain water ( $r$ ), snow ( $s$ ) or graupel ( $g$ ). In these equations, variables with a subscript 0 refer to the hydrostatic reference state, which varies in  $z$  only. The Coriolis force is simplified by omitting its component that depends on the cosine of latitude. A single prime indicates the departure from the reference state and double primes

The thermodynamic equation is given by,

where  $h$  is the moist static energy defined by  $h \equiv c_p \pi_0 \theta + Lq_v + gz$ ,  $L$  the latent heat of condensation, and  $Q_R$  and  $Q_A$  indicate the radiation and large-scale advection effects, respectively. The conservation equation for each water species is given by,

where the subscript  $x$  denotes water vapor ( $v$ ), cloud water ( $c$ ), cloud ice ( $i$ ), rain water ( $r$ ), snow ( $s$ ) or graupel ( $g$ ),  $V(\geq 0)$  the mass-weighted fall speed for precipitating particles with  $V_v = V_c = V_i = 0$ ,  $P$  the net production rate due to the microphysical processes, and  $C$  the source of cloud water and cloud ice due to condensation, deposition, evaporation and sublimation with  $C_r = C_s = C_g = 0$ .

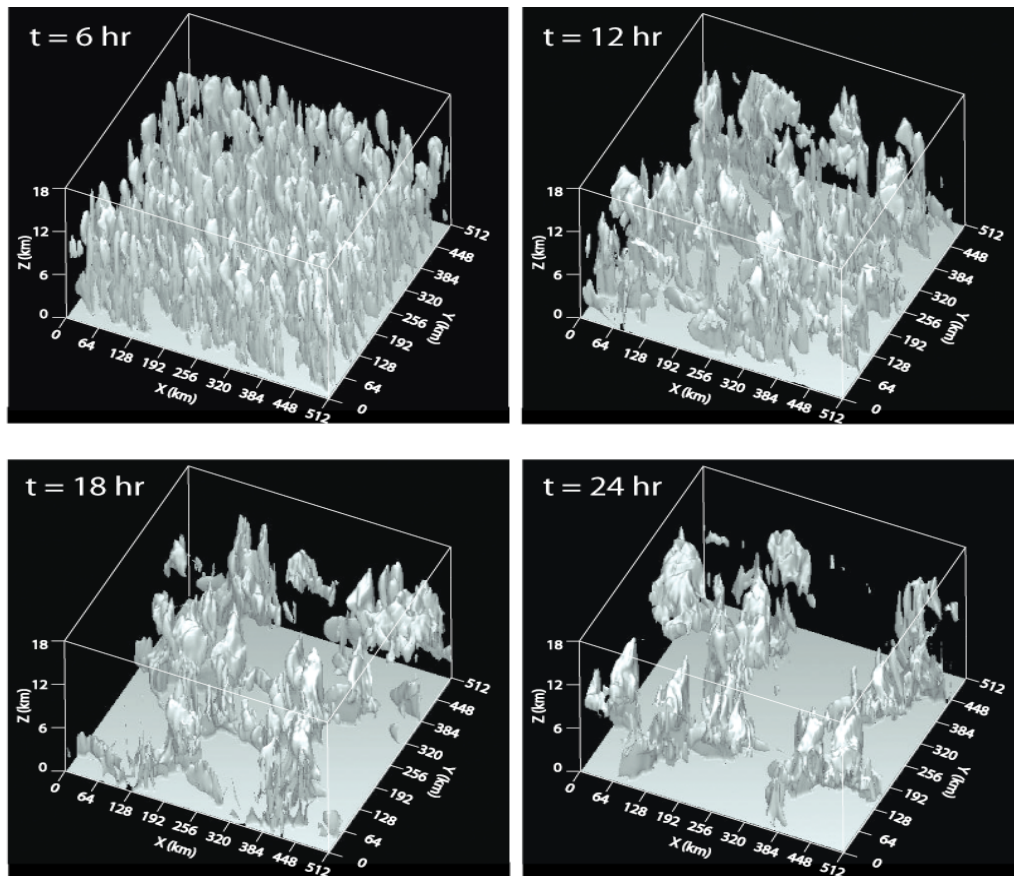


**Figure 3: Time Evolution of Isotimic Surface of Cloud Water Mixing Ratio ( $0.1 \text{ gKg}^{-1}$ ), where Cloud Water Consists of Cloud Water and Cloud Ice.**

indicate turbulence-scale velocity components. The non-dimensional pressure  $\Pi$  is given by  $\Pi = (p / p_{00})^{R/c_p}$ , where  $p$  is the pressure,  $p_{00}$  a constant reference pressure,  $R$  the gas constant for dry air and  $c_p$  the specific heat of dry air.

Here we shall illustrate simulation of the development of an ensemble of clouds using the model with full physics, which includes microphysics, radiation, and turbulence based on Jung and Arakawa (2007). The model is

applied to a 512-km x 512-km horizontal domain with a 2-km horizontal grid size. In the vertical, the model has 34 levels based on the stretched vertical grid described in section 3b with a top at 18 km. The vertical grid size ranges from about 100 m near the surface to about 1000 m near the model top. The upper and lower boundaries are rigid and the lateral boundaries are cyclic. The Coriolis parameter for 15° N is used. An idealized ocean surface condition is used, in which the surface temperature is prescribed as 299.8 K. The cosine of the solar zenith angle is fixed to 0.5, representing a typical daytime condition in the tropics. The initial thermodynamic state and zonal wind fields are selected idealizing the GATE Phase-III conditions.

Figure 3 shows development of cloud ensemble for initial 24-hour period (Jung and Arakawa, 2007). The figure shows the isotimic surface of cloud water mixing ratio ( $q=0.1 \text{ g kg}^{-1}$ ) in every 6 hours. Here cloud water consists of cloud liquid water and cloud ice. In early stage of this period, clouds develop nearly everywhere because the integration starts from a horizontally uniform and conditionally unstable condition. As time progresses, mesoscale band-like cloud organizations gradually develop, which seem to have multiple directions.

#### 4. Can We Forecast Them With Sufficient Accuracy?

The models discussed above are good for testing idealized simulations, process studies and development of new schemes. Forecasting of thunderstorm is done based on a combination of synoptic method, Doppler Weather Radar and Numerical Model products (Das et al. 2009, 2015). They are briefly summarized below.

##### 4.1 Synoptic method

###### 4.1.1 Uses of T- $\Phi$ gram

The T- $\Phi$  gram or Skew-T diagram (fig. 4) offers a way to look at the measurements made with a Radiosonde. A T- $\Phi$  gram is drawn based on observations as well as forecast

model products. The cloud layer (where dew point and temperature are the same) is determined from the T- $\Phi$  gram. Inversion layers are identified from the T- $\Phi$  gram. The Lifted Condensation Level (LCL), which is the expected cloud base height and the Level of Free Convection (LFC) where a parcel of air becomes positively buoyant is determined. The CAPE (Convective Available Potential Energy) and CINE (Convective Inhibition Energy) are also determined. Areas of instability [the layer between LFC and Equilibrium Temperature Level (ETL)], stronger CAPE ( $> 1000 \text{ J kg}^{-1}$ ) and lower CINE are the regions where development of thunderstorms are possible.

##### 4.1.2 Convective Indices

There are many convective indices such as CAPE, CINE, Lifted Index, Showalter index, Total Total index, SWEAT index, Bulk Richardson Number, etc. that are generally used for operational forecasting. These convective indices are calculated based on observed soundings as well as forecast model products.

###### *Convective Available Potential Energy (CAPE):*

The Convective Available Potential Energy (CAPE) is the positive [buoyancy](#) of an air parcel. It is the amount of [energy](#) a [parcel](#) of [air](#) would have if lifted a certain distance vertically through the atmosphere. It is an indicator of atmospheric instability. It is defined as

where,  $Z_f$  and  $Z_n$  are the levels of free convection and neutral buoyancy respectively.  $T_{vp}$  and  $T_{ve}$  are the virtual temperatures of the air parcel and environment respectively. The threshold values of CAPE for different stability regimes are given below.

CAPE < 1000 : Instability is weak

CAPE > 1000 < 2500 : Moderate instability

CAPE > 2500 : Strong instability

###### *Convective Inhibition Energy (CINE):*

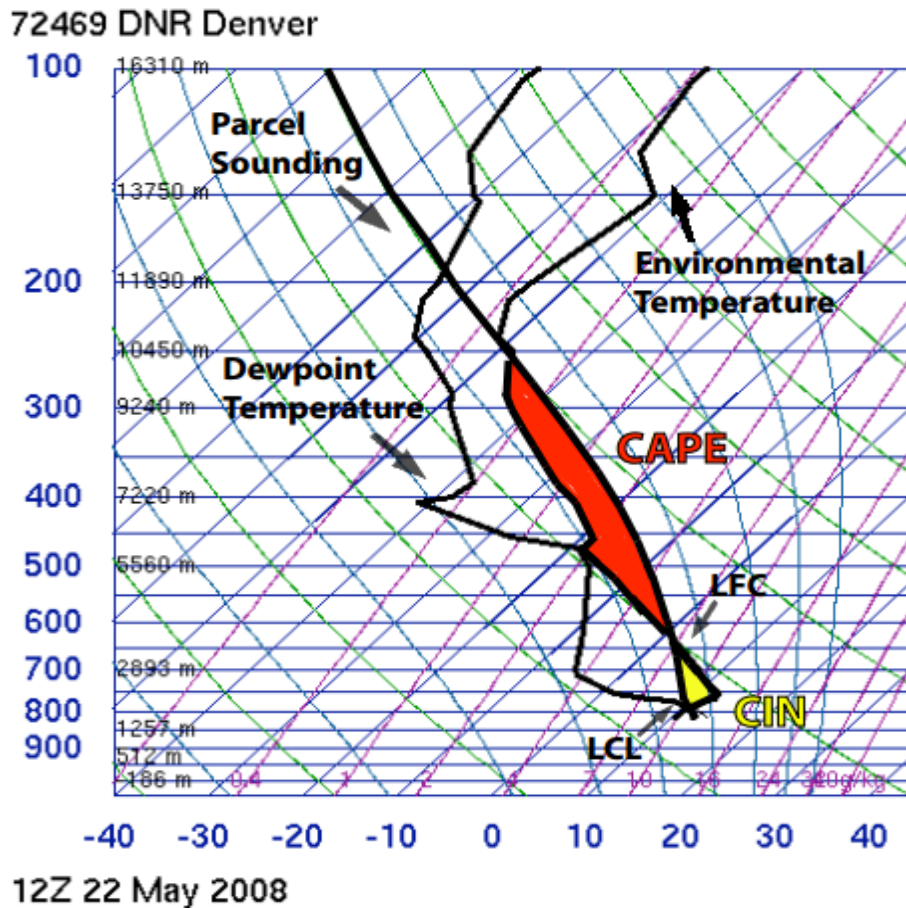


Figure 4: Illustration of a Typical Sounding on Skew-T Log-P Diagram.

CINE is a negative energy which prevents the CAPE to be spontaneously released. The negative buoyancy typically arises from the presence of a lid. If CINE is large, deep convection will not form even if other factors may be favourable. It is expressed as follows:

where,  $Z_o$  and  $Z_f$  are the levels at which parcel originates and free convection respectively.

**Lifted Index (LI):**

The Lifted index (LI) is the temperature difference between an air parcel lifted adiabatically to a given pressure (height) in the atmosphere (usually 500 hPa) and the temperature of the environment at that level. When the value is positive (negative), the atmosphere is stable (unstable). LI is generally scaled as follows:

LI = 6 or Greater: Very Stable Conditions

LI Between 1 and 6: Stable Conditions, Thunderstorms Not Likely

LI Between 0 and -2: Slightly Unstable, Thunderstorms Possible, With Lifting Mechanism (i.e., mechanical, daytime heating, ...)

LI Between -2 and -6: Unstable, Thunderstorms Likely, Some Severe With Lifting Mechanism

LI Less Than -6: Very Unstable, Severe Thunderstorms Likely With Lifting Mechanism

**Showalter Index (SI):**

The Showalter Index is defined as  $SI = T_{500} - T_{p_{500}}$ ; where  $T_{p_{500}}$  is the temperature of a parcel lifted dry adiabatically from 850 mb to its condensation level and moist adiabatically to 500 mb.



SI values  $\leq +3$  indicate possible showers or thunderstorms.

SI values  $\leq -3$  indicate possible severe convective activity.

Note that the LI differs from the SI by the initial location of the lifted parcel.

**SWEAT (Severe Weather Threat) Index:**

It is defined as,  $SWEAT = 12T_{d_{850}} + 20(TT - 49) + 2f_{850} + f_{500} + 125(s + 0.2)$ ;

where the first term is set to zero if the 850 mb Td ( $^{\circ}C$ ) is negative; TT is the Total Totals Index (if  $TT < 49$ , the term is set to zero); f is the wind speed in knots; and  $s = \sin(500 \text{ mb})$

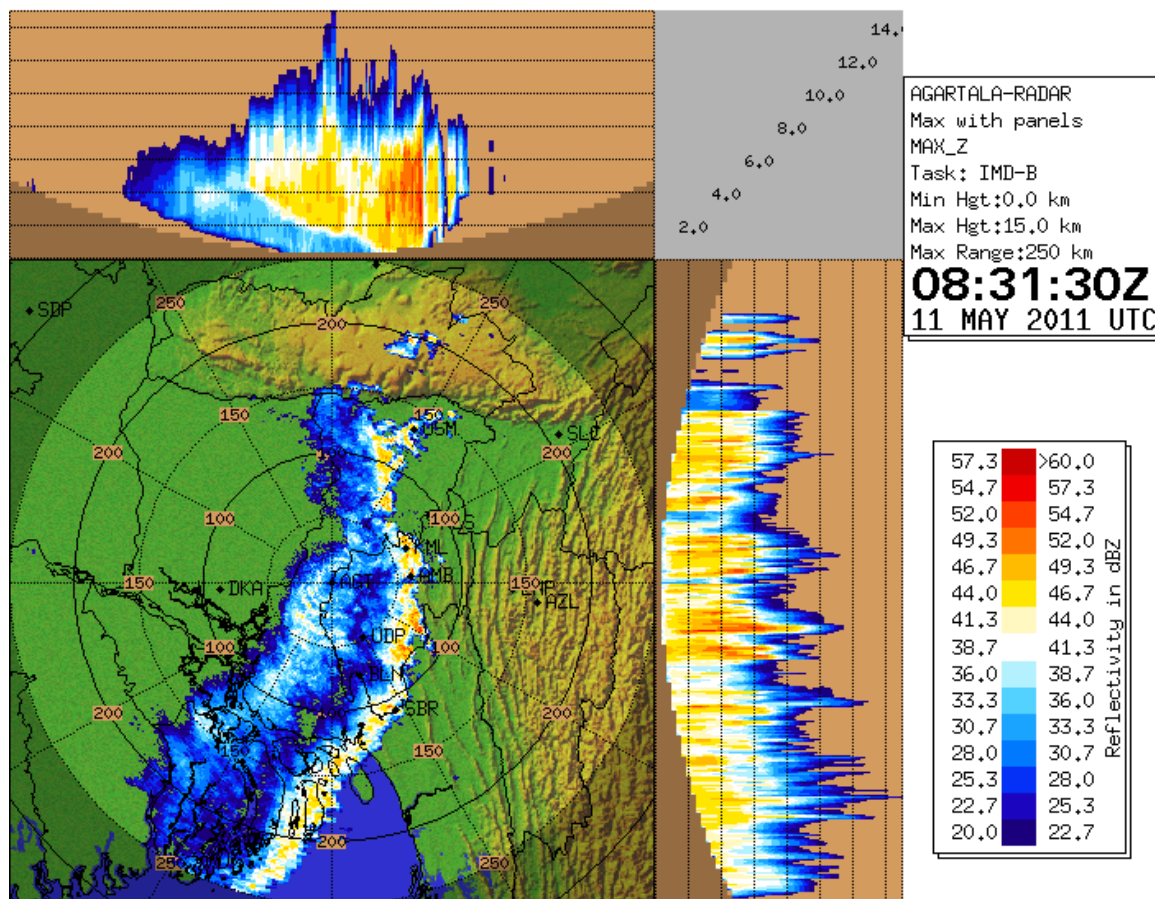


**Figure 5: A Squall Line Observed by Doppler Radar at Agartala on 11 May 2011**

**Total Total Index (TTI):**

It is defined as  $TTI = T_{850} + T_{d_{850}} - 2T_{500}$

$TTI \geq 40$  indicator of occurrence of Nor'westers

$TTI \geq 47$  indicator of severe Nor'westers with tornado intensity.

The total totals index is actually a combination of the vertical totals,  $VT = T_{850} - T_{500}$ , and the cross totals,  $CT = T_{d_{850}} - T_{500}$ , so that the sum of the two products is the total totals.

wind direction - 850 mb wind direction). The last term is set to zero if any of the following is not met:

- 1) the 850 mb wind is between  $130^{\circ}$ - $250^{\circ}$ ;
- 2) the 500 mb wind is between  $210^{\circ}$ - $310^{\circ}$ ;
- 3) (the 500 mb wind direction - the 850 mb wind direction) is greater than zero; or, both the wind speeds are greater than or equal to 15 kts.

SWEAT values  $+250$  indicate a potential for strong convection.

SWEAT values +300 indicate the threshold for severe thunderstorms.  
 SWEAT values +400 indicate the threshold for tornadoes.

Practically, its value determines whether convection is free or forced. High values indicate unstable and/or weakly-sheared environments; low values indicate weak instability and/or strong vertical shear.

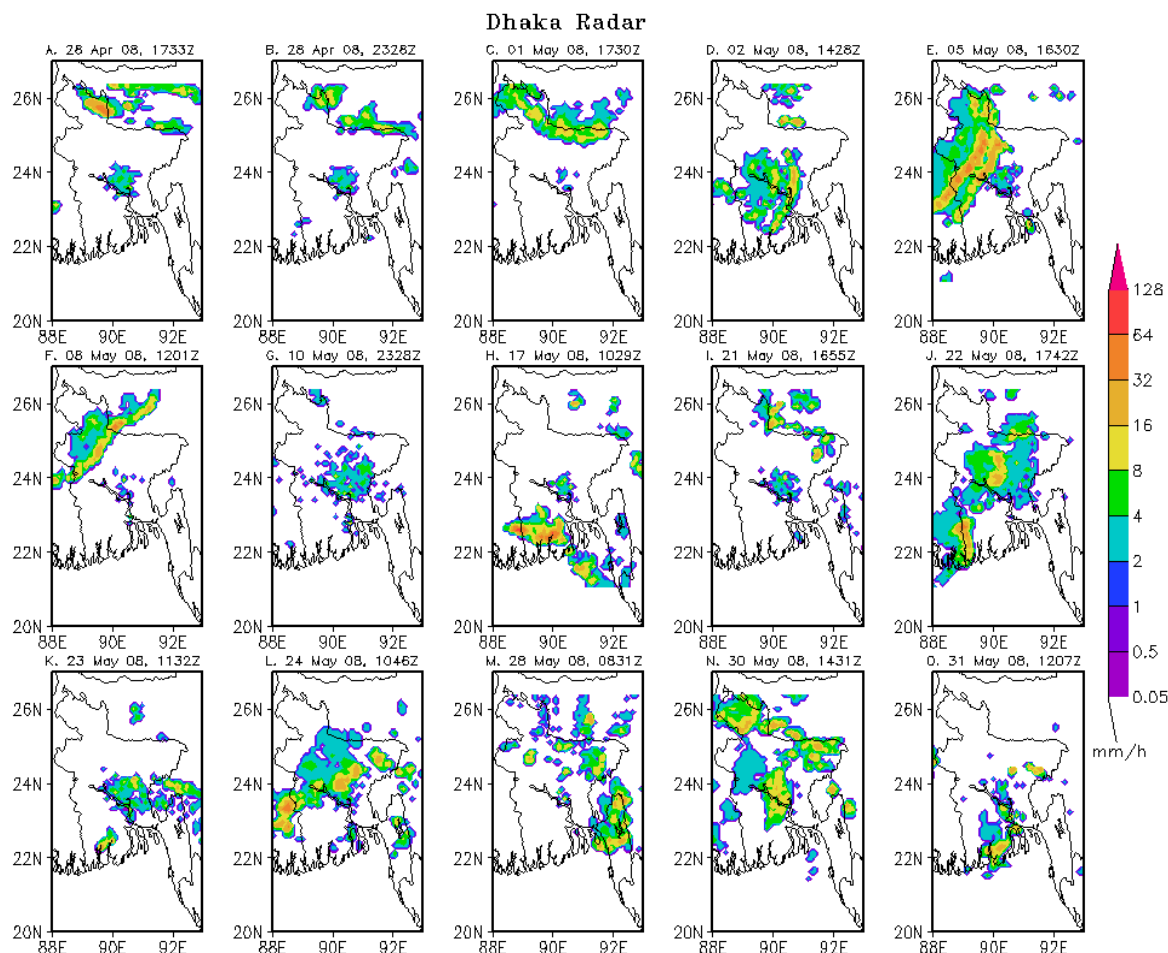


**Figure 6: Precipitation Rate (mm h<sup>-1</sup>) Retrieved from the Dhaka Radar on the Days of Nor’westers in 2008 (Reproduced from Das et al. 2015).**

It may be noted that these indices are empirical only, i.e., they are not governed by any physical laws. They are used by meteorologists to give a quick estimate of the atmospheric condition.

**Bulk Richardson Number (BRN):**

The Bulk Richardson Number (BRN) is a dimensionless number relating vertical stability and vertical shear (generally, stability divided by shear). It represents the ratio of thermally produced turbulence and turbulence generated by vertical shear.

Generally, values in the range of around 10 to 45 suggest environmental conditions favorable for supercell development. For mesoscale forecasting purposes, the Bulk Richardson Number (BRN) relates buoyancy through CAPE to vertical wind shear for a 5.5 km thickness and is simply defined as:

$$BRN = CAPE / (0.5 * (u_{6km} - u_{500m})^2)$$

Where, u<sub>6km</sub> is the wind speed at 6km above ground level (AGL) and u<sub>500m</sub> is the wind speed at 500m AGL. In summary,

BRN <10 : Probably too much shear for thunderstorms

BRN > 10 < 45 : Supercells possible

BRN > 45 : Storms more likely to be multicells rather than supercells.

indicate that winds are blowing towards the RADAR site. Doppler radars are used to monitor convergence lines even in the absence of clouds. It has been demonstrated (Wilson et al., 1998) that forecasters could often anticipate thunderstorm initiation by

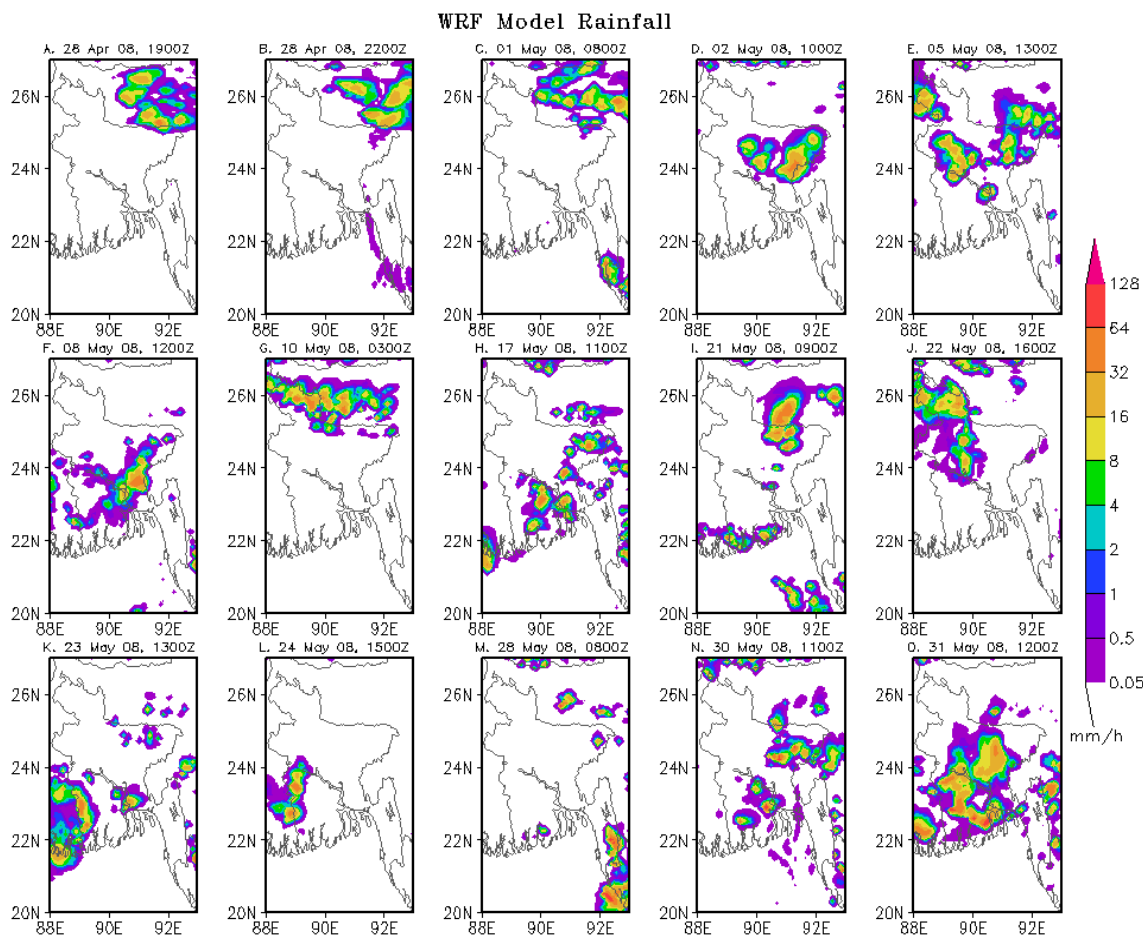


**Figure 7: Precipitation Rate (mm h<sup>-1</sup>) Simulated by the WRF Model on the Days of the Nor’westers in 2008 (Reproduced from Das et al. 2015).**

#### 4.2 Radar Detection of Thunderstorms

Doppler RADAR can detect the location and intensity of storms (reflectivity), the speed and direction of wind (velocity), and the total accumulation of rainfall (storm total). RADAR systems generate a different image for each. A reflectivity image (Fig. 5) shows the location where rain, snow, or other precipitation is falling and how intensely. Velocity images reveal the speed and direction of winds. The color keys are not standard, but on some images warm colors, like red and orange, indicate that winds are blowing away from the RADAR site. Cool colors, like green and blue,

monitoring Doppler radar-detected boundary layer convergence lines (boundaries) together with visual monitoring of cloud development in the vicinity of the convergence line. Figure 5 illustrates a squall line observed by radar at Agartala. Squall lines typically bow out due to the formation of a mesoscale high pressure system which forms within the stratiform rain area behind the initial line.

#### 4.3 Numerical Prediction of Thunderstorms

Numerical models have the ability to simulate all the phases of thunderstorm evolution. Thunderstorms are mesoscale phenomena.

Mesoscale weather systems refer to those which are smaller than synoptic scale (about 1000 km) and larger than the cumulus scale (~

First was the introduction of nonhydrostatic dynamics into mesoscale models (e.g., Dudhia 1993). The nonhydrostatic mesoscale models

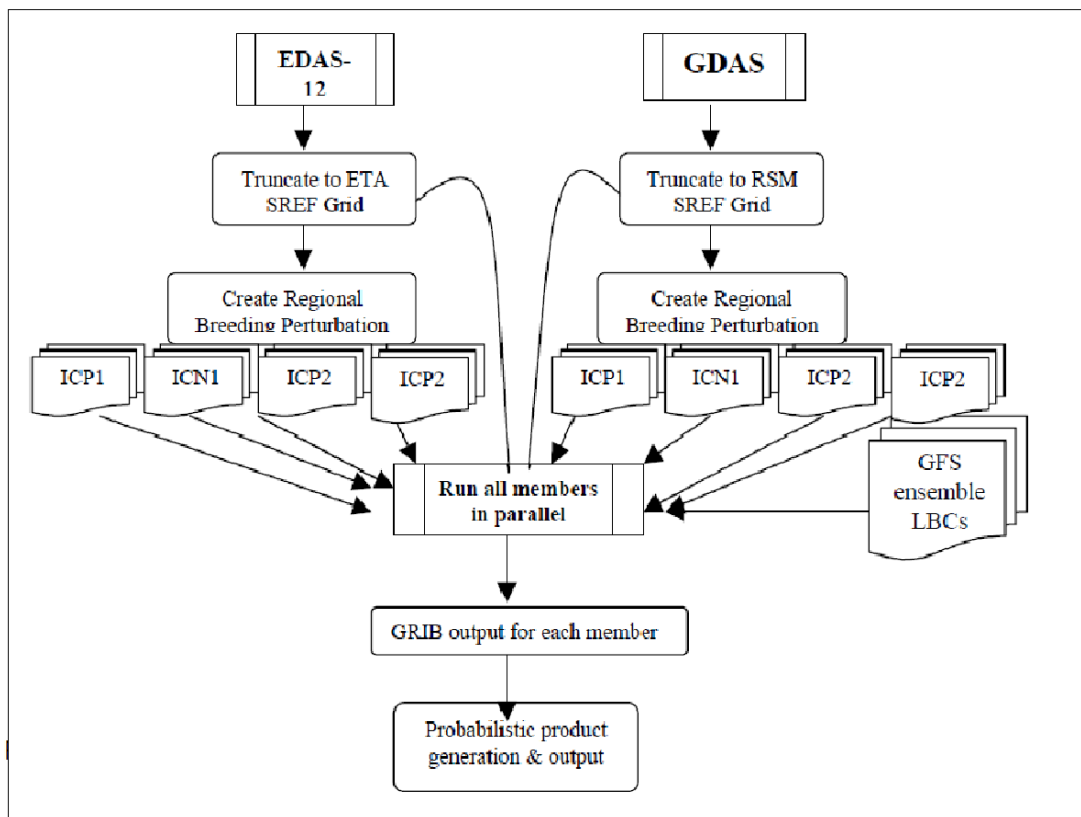


**Figure 8: Outline of NCEP SREF Operational system run (Multi-IC) in 2003. ICP, ICN, I represent Initial Condition files for the Positive and Negatively perturbed runs, respectively.**

1 km). Mesoscale models are designed for the simulation and prediction of mesoscale weather systems. Such models remain important for an operational numerical weather prediction center, because they can be run at very high resolution on a nested grid with a wide variety of options for the parameterization of physical processes. The global models do not have such privileges and, they are very expensive to run at high resolutions. Moreover, at finer resolution the mesoscale models are also capable of assimilating large amount of high resolution observations available from present day satellites and Doppler radars. The mesoscale models can be configured to run from global to cloud resolving scale for simulation of thunderstorms and cloud cluster properties. Since the early 1990s several important changes took place in mesoscale modeling.

can be run at cloud resolving resolutions (~1 km) without the restrictions of the hydrostatic assumption. This greatly increases the range of scientific problems to which the models can be applied. For example, at such resolution, mesoscale models can explicitly simulate convection and its interaction with the larger scale weather systems in a realistic way. However, the use of high-resolution mesoscale models for real-time NWP requires a tremendous amount of computational resources. Presently, mesoscale models have been developed with a wide varieties of flexibilities in terms of changing horizontal and vertical resolutions, nesting domains, and choosing options for different physical parameterization schemes, i.e. MM5, WRF, RAMS, ETA, ARPS, HIRLAM, etc (Anthes, 1990; Dudhia, 1993; Cotton et al, 1994; Mesinger, 1996; Toth, 2001, Case et al.,

**Table 2: Composite characteristics**

Sl. No.	Name	Observation	Model
1.	Cloud Top Altitude (km)	13.14	15.19
2.	Altitude of Core precipitation (km)	3.55	4.5
3.	Intensity of Core precipitation ( $\text{mm h}^{-1}$ )	32.0	182.93
4.	Precipitation rate at Surface ( $\text{mm h}^{-1}$ )	29.67	61.93
5.	Direction of movement ( $^{\circ}$ )	293	263
6.	Speed of movement ( $\text{km h}^{-1}$ )	47.78	48.7
7.	Maximum wind speed at surface ( $\text{m s}^{-1}$ )	20	13.85
8.	Length of Squall line (km)	186.27	271.39
9.	Updrafts speed (max), $\text{m s}^{-1}$	20	7.18
10.	Downdrafts speed (max), $\text{m s}^{-1}$	8	1.4
11.	Total Cloud Hydrometers (max), $\text{g m}^{-3}$	3.5	3.25

2002). These models require initial and boundary conditions from a large-scale/ global model and may be used for forecasting up to 72 hours. Such models can be run at cloud resolving scale for simulation of thunderstorms and cloud cluster properties.

Das et al. (2015) studied several cases of Nor'westers that formed over northeast India and adjoining Bangladesh region during the pre-monsoon season employing observations from ground based radar, Tropical Rainfall Measuring Mission (TRMM) and synoptic stations. Subsequently, they made an attempt to simulate the storms using Weather Research and Forecasting (WRF) model. Figure 6 depicts the precipitation rates retrieved from the Dhaka radar of BMD for different thunderstorm days. The storms were classified based on the radar echo patterns (Bluestein and Jain, 1985; Houzeet *et al.*, 1990; Parker and Johnson 2000; and Grams *et al.*, 2006). It is found that almost all Nor'westers (light, moderate and severe) can be classified as

embedded areal (EA; 9 out of 10 cases) based on the definition of Bluestein and Jain (1985). Almost all the squall lines belong to the broken areal category (BA; 5/ 5 cases). Further, following the classification of Parker and Johnson (2000), it is found that almost all the Nor'westers as well as the squall lines of East/ Northeast India and Bangladesh belong to the trailing and parallel stratiform (TS/ PS) categories. TS type squall-line is more common in this region (Dalalet *et al.*, 2012). Precipitations were simulated by the model (Figure 7) for all the observed cases presented in Figure 6. The model shifted the areas of precipitations both in time and locations. But the intensities of the precipitation rates are simulated very well. The model simulated the storms generally 3-4 hours ahead of the observations.

Das et al (2015) determined the composite characteristics of Nor'westers based on the observations and simulations of the 15 cases of severe, moderate and light thunderstorms. The

composite characteristics are presented in Table 2. There are differences between simulations and observations. The table indicates that the depths of the clouds are about 12-15 km. The model slightly overestimated the depth of cloud, altitude and intensity of core precipitation. While there are much subjectivity involved in retrieving the values from model and observations, notable among the features is that both observations and the simulation showed the direction of movement of the storms from northwest. The model severely underestimated the wind speed at surface. The propagation speeds of the storms were  $47.78 \text{ km h}^{-1}$  (observed) and  $48.70 \text{ km h}^{-1}$  (simulated). Average lengths of the squall lines were about 186 km (observed) and 271 km (simulated). The average updraft and downdraft strengths simulated by the model in this study are about  $7.18 \text{ m s}^{-1}$  and  $1.4 \text{ m s}^{-1}$  respectively. Total amounts of hydrometeors simulated inside the Nor'westers are about 3 to  $3.5 \text{ g m}^{-3}$ . Their study also suggested that many of the long lived squall lines originated in India and travelled across Bangladesh in the form of two parallel bows. The squall line had length of about 200 km. The rear bow appeared stronger than the leading one. The two parallel bands of rainfall; the primary and the secondary bands with an area of low rainfall between the two bands are clearly seen from the radar echoes. Such features are also reported over West Bengal, India (Dawn and Mandal, 2014).

#### 4.4 Ensemble Forecasting Method of Thunderstorm and Lightning Strike

A single model may not be able to forecast accurately. Hence, for operational forecasting several models are run at one time – an ensemble. If each run produce similar outputs, the probability of the model forecast of an event is highest. If the runs look different, the probability of the model forecast is low. Another technique is to run the same model several times with varying initial weather conditions. This approach results in a number of predictions that produce a range of possible future weather outputs.

Probably the first real time regional ensemble prediction system was implemented at NCEP in 2001 (Bright et al., 2009) based on a 10-member Short-Range Ensemble Forecasting (SREF). The NCEP-SREF emphasizes on both initial conditions (IC) and physics uncertainties. It uses multi-analyses (EDAS and GDAS), multi LBCs (using NCEP global ensemble members), multi-model (Eta and RSM) and perturbing ICs (breeding approaches). Presently, the SPC (Storm Prediction Centre) SREF is constructed by post-processing 21 members of the NCEP SREF plus the 3-hour time lagged, operational WRF-NAM (for a total of 22 members) each 6 hours (03, 09, 15, and 21 UTC). Output is available at 3h intervals through 87 hours. The SPC ensemble post-processing focuses on diagnostics relevant to the prediction of SPC mission-critical high-impact, mesoscale weather including: thunderstorms and severe thunderstorms, large scale critical fire weather conditions, and mesoscale areas of hazardous winter weather. Figure 8 outlines the SREF forecast system run process.

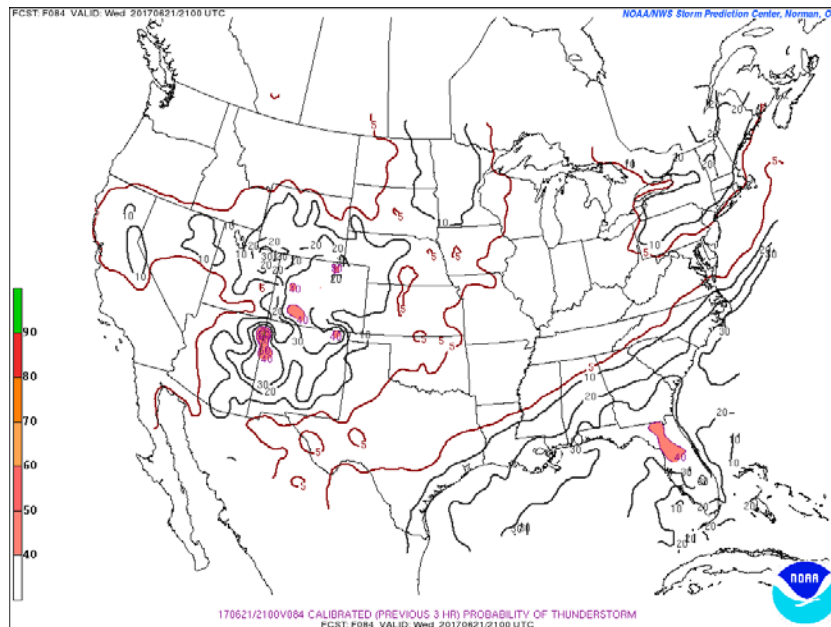
Bright et al. (2005) and Bright and Grams (2009) provide information on the SPC-SREF thunderstorm calibration technique with detailed verification results that show the forecasts to be both reliable and skilful. An example is shown in Fig 9 for the 18 hour SREF calibrated thunderstorm and lightning ( $\geq 100 \text{ CG}$ ) strikes forecast for the three hour period ending at 21 UTC 21 June 2017. Bright et al (2005) defined a Cloud Physics Thunder Parameter (CPTP) based on the (1) temperature at LCL ( $\geq -10^0 \text{ C}$ ) to ensure presence of super cooled liquid water, (2) temperature at equilibrium level ( $\leq -20^0 \text{ C}$ ) to ensure the cloud top is above the charge reversal zone, and (3) CAPE in the 0 to  $-20^0 \text{ C}$  layer  $\geq 100$  to  $200 \text{ J kg}^{-1}$  to ensure existence of sufficient vertical motion in mixed-phase region through the charge reversal temperature zone.

### 4.5 Rapid Update Cycle Data Assimilation

The first attempt to initialize a cloud-scale numerical model using radar observations for the simulation of a thunderstorm was made by

rainwater from radar reflectivity observations were used to initialize a cloud-resolving numerical model. Sun and Crook (1997, 1998) developed a four-dimensional variational data assimilation (4DVAR) scheme for the

(a)



(b)

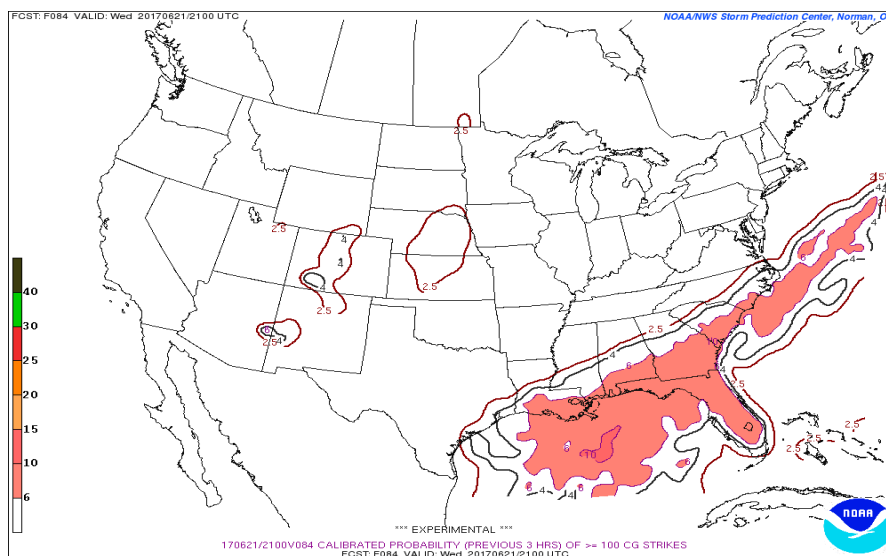


**Figure 9: The forecast probability of (a) thunderstorm and (b)  $\geq 100$  CG lightning strike from the NCEP SREF model. The forecast is valid for the 18 to 21 UTC period. This 18h deterministic forecast is based on the IC of the 03 UTC on 21 June 2017.**

Lin et al. (1993). In their study, wind from a dual-Doppler analysis, temperature and pressure from a thermodynamic retrieval, and

initialization of a cloud-scale model with single-Doppler radar observations. Sun (2005) further explored the feasibility of numerical

weather prediction of convective storms using detailed high-resolution observations from single-Doppler radar and the 4DVAR scheme developed by Sun and Crook (1997) based on Variational Doppler Radar Analysis System (VDRAS) for a real-data case of a supercell storm. The dry version of VDRAS has been implemented in a number of field projects, including the WMO Sydney 2000 Olympic Project (Crook and Sun 2002) and the Beijing 2008 Forecast Demonstration Project (B08FDP) in support of the Beijing Summer Olympics (Sun et al., 2010), to produce real-time low-level wind analysis for nowcasting of thunderstorms.

Although the fundamental data assimilation theory does not depend on the scale of interest, convective-scale data assimilation possesses a number of important differences from the large-scale. First, the main objective of the convective-scale data assimilation for NWP is to improve QPF, while the major concern for the large-scale is to reduce the error in the prediction of the 500 hPa geopotential height. Second, the major observational data source for the convective scale is from Doppler radar (although other observations are also important) while radiosonde and satellite observations are indispensable for the large scale. Third, the model constraints are different: for the large scale, balance constraints, such as geostrophic balance, are good approximations to the full set of atmospheric equations; however, for the convective scale, there are no simple balances and approximations, other than the full set of model equations describing the convective-scale motion. Lastly, synoptic-scale dynamics are quasi-linear (except for subgrid-scale parametrization) for approximately 6 hours (Gilmour *et al.* 2001) while the time-scale of a developing thunderstorm can be as short as a few minutes. Because of this number of differences, the implementation of data assimilation methods for the convective scale can be different from the large scale.

The techniques that have been applied to convective-scale assimilation are, (1) Single-Doppler retrieval and direct insertion of retrieved fields, (2) Successive correction, (3) Three-dimensional variational (3D-Var) technique, (4) 4D-Var, and (5) Ensemble Kalman Filter. The issues with the convective

scale data assimilation are, (1) Processing Radar Data, (2) Combining Radar data with other types of observations, (3) Cycling frequency, (4) Nonlinearity in microphysics, (5) Single and Multiple Doppler Synthesis, (6) Estimation of observation and forecast errors, (7) Using Polarimetric Radar information, and (8) Low-level moisture and land-surface data assimilation. Details of these techniques may be referred from Sun et al. (2010), and Benjamin et al. (2016). Presently, NCEP uses an hourly updated assimilation and model forecast system called the Rapid Refresh (RAP) - Benjamin et al. (2016). It replaced the Rapid Update Cycle (RUC) in 2012. The RAP uses the Advanced Research version of the WRF-ARW and the Gridpoint Statistical Interpolation analysis system (GSI). RAP forecasts are generated every hour with forecast lengths going out 18 hours. Multiple data sources go into the generation of RAP forecasts including commercial aircraft weather data, balloon data, radar data, surface observations, and satellite data.

**Table 3:** Sensitivity experiments using different combinations of physical parameterizations

S.N.	Combination of Cloud microphysics, Convection and PBL schemes	Options
Expt-1	Lin, KF, YSU	m2c1p1
Expt-2	WSM3, KF, YSU	m3c1p1
Expt-3	WSM6, KF, YSU	m6c1p1
Expt-4	Milbrandt, KF, YSU	m9c1p1
Expt-5	Milbrandt, BMJ, YSU	m9c2p1
Expt-6	Milbrandt, GDE, YSU	m9c3p1
Expt-7	Milbrandt, GDE, MYJ	m9c3p2
Expt-8	Milbrandt, GDE, ACM2	m9c3p7
Expt-9	Milbrandt, No-cumulus, YSU	m9c0p1



### 5. What is the Skill of Forecasts?

Predicting the track of the movement of thunderstorm and its intensity by using a numerical model and quantify the skill of the model in predicting time and location of occurrence and the intensity poses a big challenge. As discussed earlier, a single

schemes (namely; Kain-Fritsch, Betts-Miller-Janjic, Grell-Devenyi and no-cumulus), cloud microphysics schemes (namely; Lin *et al.*, WSM3, WSM6 and Milbrandt), and planetary boundary layer schemes (namely; YSU, MYJ and ACM2) to examine the root mean square errors (RMSE) of forecasts. The NOAA

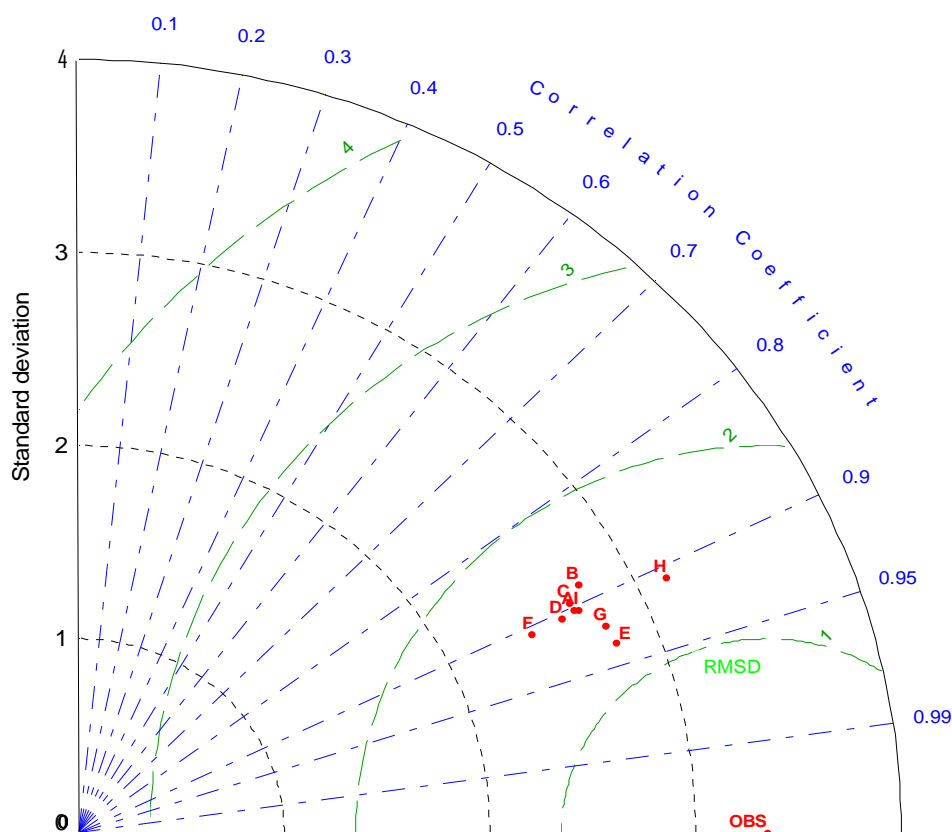


**Figure 10a: Taylor diagram for temperature obtained from all simulated cases. This diagram summarizes the correlation coefficient, root mean square difference (RMSD) and standard deviation of the model simulation with respect to the observation. The character A, B, C, D, E, F,G, H and I represents m2c1p1, m3c1p1, m6c1p1, m9c1p1, m9c2p1, m9c3p1, m9c3p2, m9c3p7 and m9c0p1 respectively (as summarized in Table 3)**

deterministic model may not be able to provide skillful forecasts. Therefore, ensemble forecasting based on multi-models, multi-physics, multi-ICs and multi-LBCs are used for obtaining skillful forecasts. In this section, we review the skill scores based on multi-physics configurations of the WRF model results described in the section 4.2.

Several sensitivity experiments were conducted by Das et al. (2015) with different combinations of cumulus parameterization

scheme was used for land surface processes in all the experiments. Table 3 summarizes the experiments. Figures 10a and 10b shows the Taylor and Box-Whisker diagrams based on all the experiments. The Taylor and Box-Whisker diagrams are made based on the 3 hourly observations of temperature and rainfall from the BMD stations and the model simulations obtained from the 9 experiments listed in the Table 3. The Taylor diagram summarizes the statistical measures for

correlation coefficient, root mean square difference (RMSD) and standard deviation. Figure 10a shows that the option m9c2p1 has highest correlation coefficient between model and observations, lowest RMSD and reasonable standard deviation compared to other options in simulation of temperature studied in this analysis. Therefore, model

therefore they decided to use m9c0p1 option in WRF to simulate the thunderstorms. Thus, they obtained the best skill scores using the combinations of no-cumulus, Milbrandt and YSU schemes (Das et al., 2015).

In the past, the determination of several verification scores were the most common

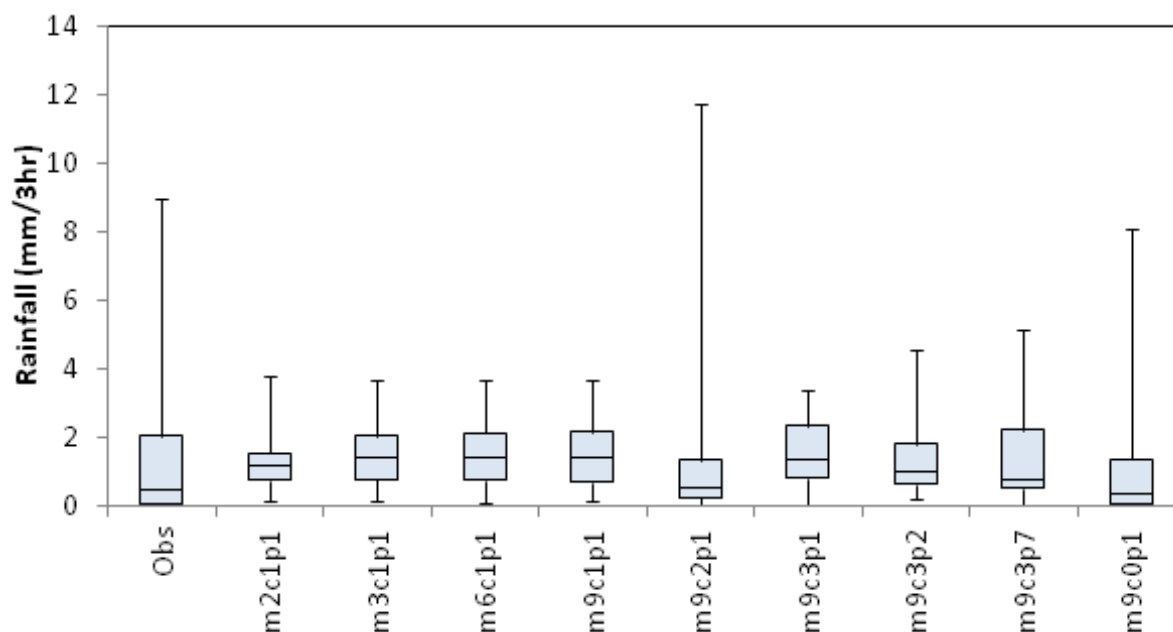


**Figure 10b: Box-Whisker plot for rainfall obtained from all simulated cases. The box indicates the lower and upper quartiles (inter-quartile range) and the horizontal line inside the box is the median of the data time series. Whiskers are the two lines outside the box that extend to the highest and lowest data values**

option m9c2p1 can be considered for the temperature simulation, but in general temperature is albeit a stable parameter to simulate homogeneous field using any climate model. On the other hand, m9c0p1 option is in the middle range in simulation of temperature but this option is found better in simulation of rainfall as shown in Figure 10b. In the Box-Whisker plot, a non-parametric statistic, the median marked by horizontal line inside the box for m9c0p1 is closer to the observation and the spread of rainfall data for upper and lower quartiles bounded by the box is also reasonable for m9c0p1. Importantly, the Whiskers are the two lines outside the box that extend to the highest and lowest data values for m9c0p1 is much closer to the observations. Because simulation of rainfall using a mesoscale model is more challenging task compared to simulation of temperature,

practice and the interpolated gauge measurements served as the verification data. These techniques are often marked as "traditional verification methods". They include the use of contingency table and the skill scores derived from the table or scalar error measures, like RMSE. The development of new verification methods started about ten years ago and was motivated by development of NWP models with high temporal and spatial resolutions, ensemble forecasting and data from radar and satellite measurements (e.g. Ebert and McBride, 2000; Casati et al, 2004, 2008; Ebert, 2008; Gilleland et al, 2009, Srivastava et al, 2010, Roy Bhowmik et al, 2011). As higher-resolution numerical models are now used to predict highly discontinuous fields, like convection, there is an increasing need of newer verification techniques (Casati et al. 2008; Gilleland et al. 2009). Newer

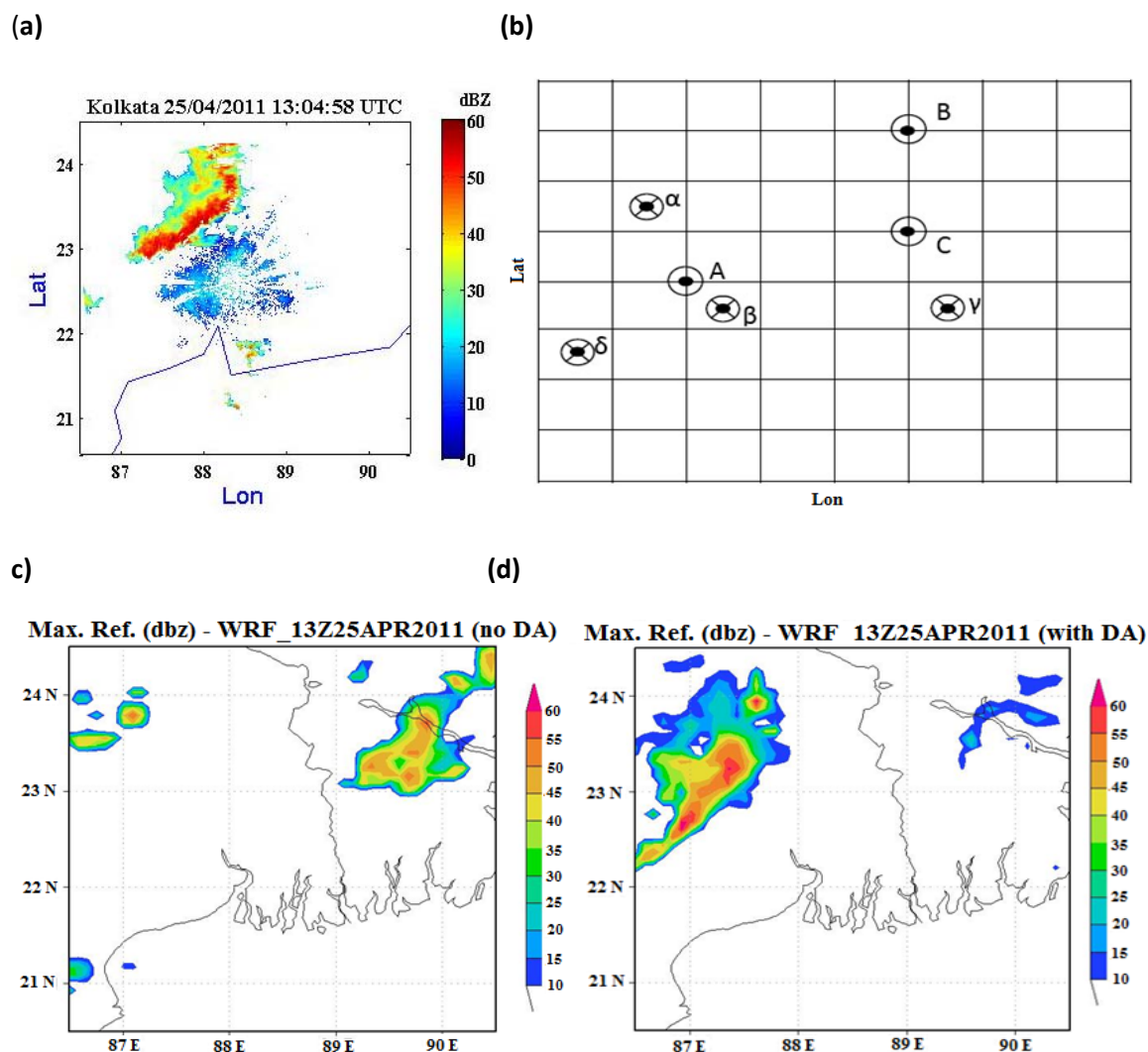


**Figure 11: (a) MAXdBZ obtained from DWR at 13:04:58 UTC, (b) Computation of Spatial Skill of the Model, (c) Model Simulated maxdBZ at 13:00 UTC of Exp-1, (d) Model Simulated maxdBZ at 13:00 UTC of Exp-2. The Points A, B, C at the Grid Points represent the Location of the Model Simulated maxdBZ value greater than 20 dBZ. The points  $\alpha$ ,  $\beta$ ,  $\gamma$ ,  $\delta$  represent the Location of the points with maxdBZ value greater than 40 dBZ as Observed by DWR.**

verification techniques that attempt to better characterize model skill for discontinuous fields can be classified into one of four categories: neighborhood (or fuzzy), scale-separation (or decomposition), feature based (or object based), and field deformation techniques (Gilleland et al., 2009). Robert and Lean (2008) presented a spatial verification score where they directly compare fractional coverage of precipitation area over a certain threshold with areas surrounding observations and forecast. The traditional verification scores are often not appropriate measures of skill for high-resolution model forecasts of

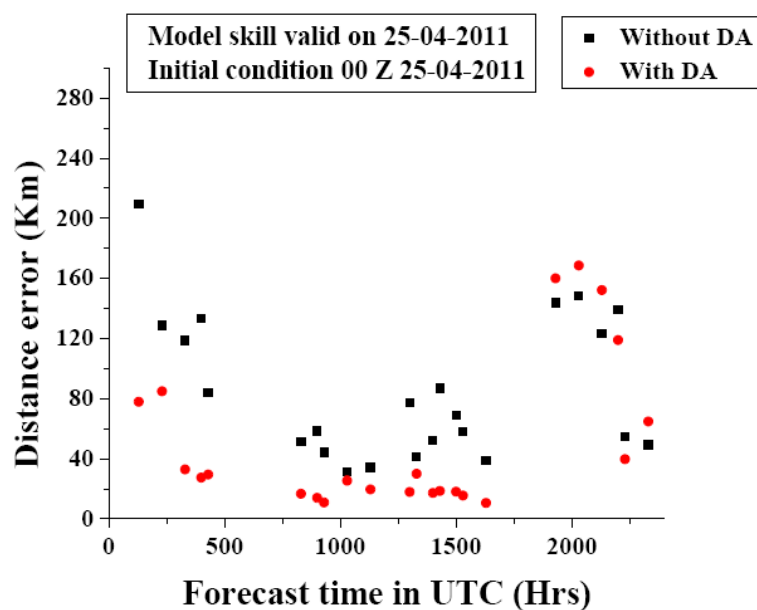
discontinuous fields (Gilleland et al. 2009), like strong convection.

Most of the past studies (Litta et al., 2012; Das et al., 2015; Karmakar, 2001; Karmakar and Alam, 2005, 2006, 2007; Prasad, 2006; Yamane et al., 2009a, 2009b; Yamane and Hayashi, 2006; Tyagi, 2007) calculated the skills of forecasting thunderstorms by comparing observations reported at discrete observatories. However, the thunderstorms may not always pass over the observing stations. A numerical model may forecast storm cells in regions where there are no observatories. Such cells are detected only by the DWRs. Hence, the skill scores computed

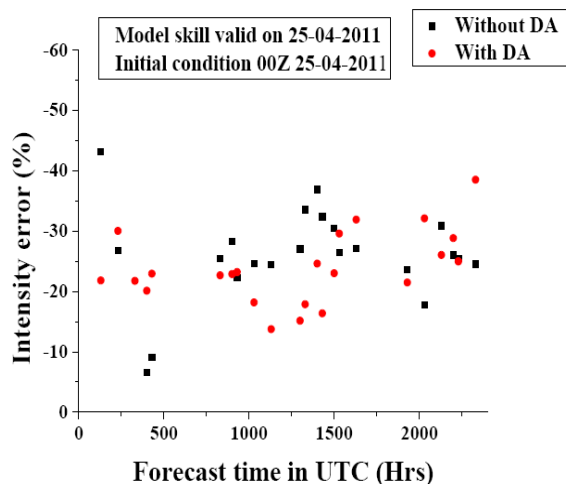
based only on the station observations may not be accurate. Sarkar et al. (2016) used a new approach to evaluate model skill in determining the location, time and intensity of a thunderstorm. The intensity skill score are measured by comparing model derived

Radar and those simulated by the WRF model for the case of a thunderstorm that occurred on 25 April 2011 at Kolkata (Sarkar et al., 2016). The 2 experiments (Expt-1 and Expt-2) shown on the diagram (Figure 11c and 11d) indicate simulations with and without data assimilation

(a)



(b)



(c)

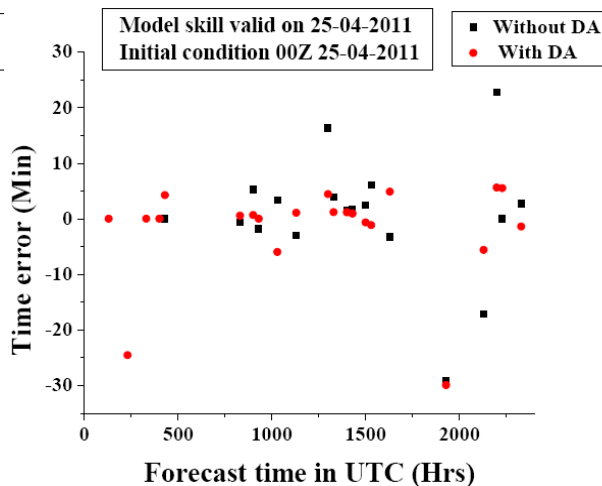


**Figure 12: Scattered plots of (a) distance error, (b) Intensity error and (c) time error for Exp – 1 and Exp-2.**

reflectivity with the reflectivity data of DWR.

For illustration Figure 11 depicts the reflectivity observed by the Doppler Weather

reflectivity. The time series of spatial, temporal and intensity errors in the forecasts are shown in Figure 12. Their results based on 5 cases of thunderstorms indicated that the

spatial errors were less than 40 km, temporal errors were  $\pm 30$  minutes and intensity errors were about -25 % (underestimated) in 24 hours.

## 6. Field Experiments on Thunderstorms

As the observation technology is improving rapidly, field campaigns are frequently organized to collect intensive observations of storms. Field observations of severe weather phenomena are collected to improve our understanding of their structures and life cycles and develop better models for forecasting the events. Over the years several field experiments have been conducted both over the Indian region and outside. IMD had conducted three field experiments during 1929 to 1941 to study the outbreak of severe convective storms (IMD, 1944; Tyagi et al., 2012). A number of field experiments have been conducted since then in USA and elsewhere (Table-5) to understand and predict the convective storms.

Realizing the importance of the pre-monsoon

Two pilot experimental campaigns were conducted during the premonsoon seasons (April–May) of 2006 and 2007 (Mohanty et al. 2006, 2007). However, the weather knows no political boundaries. Since the neighboring South Asian countries are also affected by the Nor'westers, the STORM program was expanded to cover the South Asian countries under the South Asian Association for Regional Cooperation (SAARC) in 2009 (Das et al., 2014). The STORM program covered all the SAARC countries in three phases (Figure 13). In the first phase, the focus was on Nor'westers that form over the eastern and northeastern parts of India, Bangladesh, Nepal, and Bhutan. In the second phase, the dry convective storms/dust storms and deep convection that occur in the western parts of India, Pakistan, and Afghanistan were investigated. Similarly, in the third phase, the maritime and continental thunderstorms over southern parts of India, Sri Lanka, and Maldives were investigated. Thus, overall the SAARC STORM program covered investigations about formation, modeling, and forecasting, including nowcasting of severe

**Table 4: Field Experiments related to Thunderstorms over Indian region**

S.N.	Experiment	Details	Year	Location
1	STORM	To study Nor'westers over	1929-1941	East India
2	STORM	Severe Thunderstorms Observations & regional Modeling	2006-2007	East & NE India
3	SAARC-STORM	South Asian Association for Regional Cooperation - STORM	2009-2015	South Asian region

Thunderstorms and their socioeconomic impact, the India Department of Science and Technology started the nationally coordinated Severe Thunderstorm Observation and Regional Modeling (STORM) program in 2005. It is a comprehensive observational and modelling effort to improve understanding and prediction of severe thunderstorms (STORM 2005). The STORM program is a multiyear exercise and is quite complex in the formulation of its strategy for implementation.

convective weather in the premonsoon season over South Asia. Pilot field experiments were conducted during 1–31 May of 2009–14 jointly with the SAARC countries. The programme was put on hold after the closure of the SAARC Meteorological Research Centre, Dhaka in 2015. The SAARC STORM programme is hibernating at present, but is continued as annual exercise within India during the pre-monsoon season.

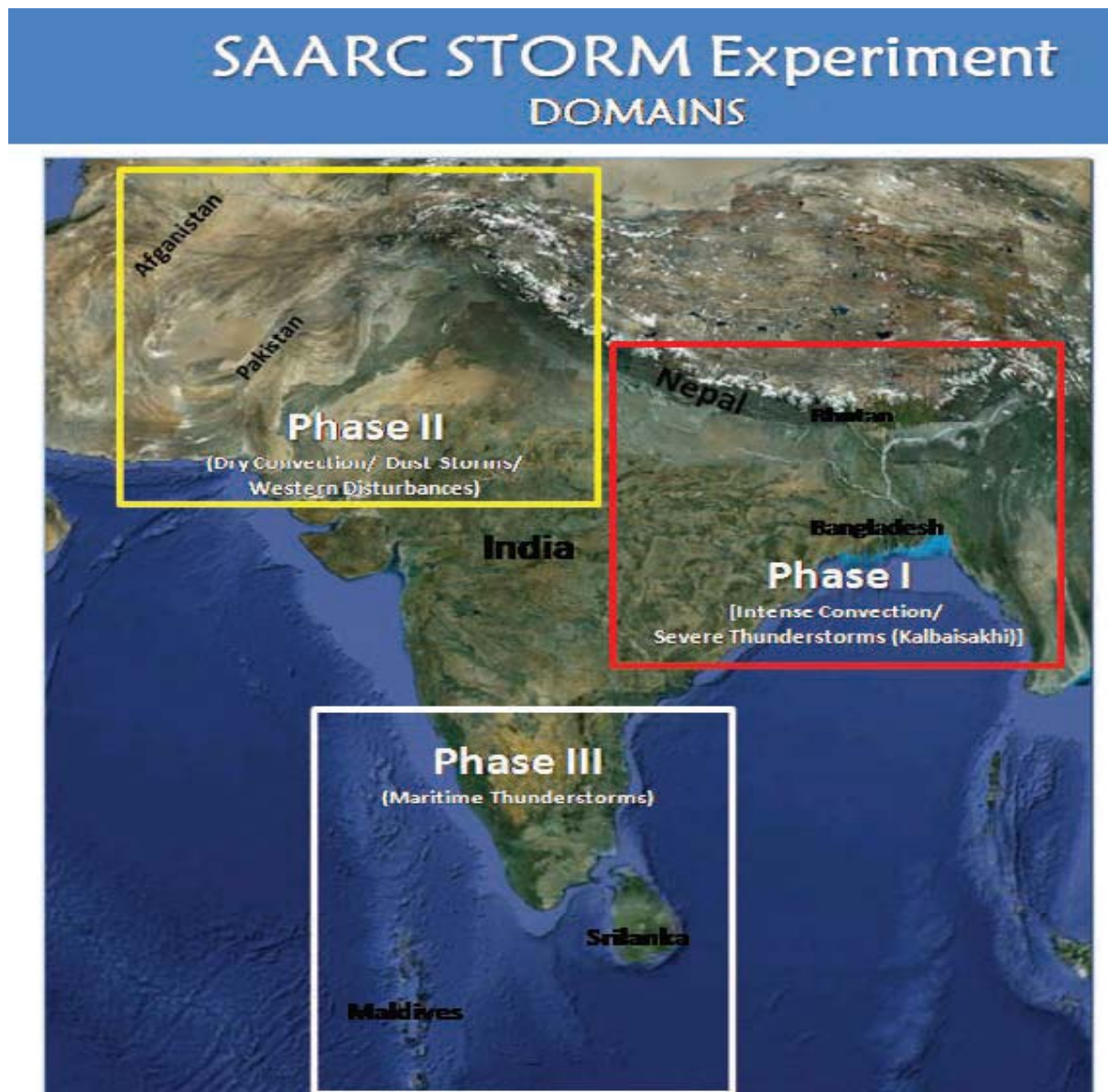


**Figure 13: The South Asian Countries in Alphabetical Order: Afghanistan, Bangladesh, Bhutan, India, Maldives, Nepal, Pakistan, and Sri Lanka, which participated in the SAARC STORM Programme**

Some of the most important experiments conducted on thunderstorms in USA are the VORTEX, BAMEX, and TELEX among others (Table 5).

The VORTEX project began in 1994, with the objective of explaining how tornadoes form (Wurman et al., 2012). The two-year field project resulted in ground-breaking data collection and led to several follow-up studies in the late 1990's. The VORTEX2 field project debuted in 2009 and continued through Spring 2010, with scientists hoping to understand

how, when, and why certain supercells produce tornadoes. In 2016, NSSL researchers embarked on VORTEX Southeast, the latest field project to examine tornadic storms. In this research program, scientists sought to understand how environmental factors in the southeastern United States affect the formation, intensity, structure, and path of tornadoes in the region. That was also the first VORTEX experiment to emphasize societal impact, with social scientists studying how the community receives and responds to warnings.

**Table 5. Field Experiments related to Thunderstorms in USA & Outside**

S.N.	Experiment	Details	Year	Location
1	EPIC	Environmental Profiling And Initiation Of Convection	2017	Oklahoma, USA
2	VORTEX SE	Verification Of The Origins Of Rotation In Tornadoes Experiment-Southeast	2016–2017	Southeastern USA
3	PECAN	PLAINS ELEVATED CONVECTION AT NIGHT	2015	Oklahoma, Kansas and Nebraska, USA
4	MPEX	MESOSCALE PREDICTABILITY EXPERIMENT	2013	USA
5	DC3	Deep Convective Clouds and Chemistry	2012	Colorado, Texas, Oklahoma, Alabama, USA
6	DYNAMO	Dynamics of the Madden-Julian Oscillation experiment	2011	Equatorial Indian Ocean
7	MC3E	Mid-latitude Continental Convective Clouds Experiment	2011	USA
8	SWCO	Southwest Colorado Radar Project to collect data on thunderstorm rainfall	2010	Colorado, USA
9	VORTEX2	Verification of the Origins of Rotation in Tornadoes Experiment	2009-2010	USA
10	PASSE	Phased-array SMART-R Spring Experiment collected data on supercell storms at low altitudes	2007	USA
11	TELEX	Thunderstorm Electrification and Lightning Experiment	2003-2004	USA
12	BAMEX	Bow Echo and MCV Experiment	2003	
13	CRYSTAL-FACE	Cirrus Regional Study of Tropical Anvils and Cirrus Layers - Florida Area Cirrus Experiment	2002	USA
14	IPEX	Intermountain Precipitation Experiment to study structure and evolution of winter storms	2000	Utah, USA
15	STEPS	Severe Thunderstorm Electrification and Precipitation Study	2000	High Plains, USA
16	VORTEX	A small follow-on project to the original VORTEX	1999	USA
17	MEAPRS	MCS Electrification and Polarimetric Radar study designed to investigate electrification in mesoscale convective systems	1998	Oklahoma-Texas-Kansas, USA
18	TIMEX	Thunderstorm Initiation Mobile Experiment	1997	USA
19	VORTEX	Verification of the Origins of Rotation in Tornadoes Experiment	1994-1995	USA
20	TOGA-COARE	Tropical Ocean Global Atmosphere (TOGA) Coupled Ocean Atmosphere Response Experiment (COARE)	1992-1993	West Pacific
21	COPS	Cooperative Oklahoma Profiler Studies to sample tornadic supercells.	1991	Oklahoma, USA
22	TAMEX	Taiwan Area Mesoscale Experiment	1987	Taiwan
23	PRE-STORM	Preliminary Regional Experiment for STORM-Central for Mesoscale Convective Systems.	1985	USA
24	TOTO	TOrnado Observatory to deploy in the tornado path collect data	1981-1984	USA
25	SESAM	Severe Environmental Storm and Mesoscale Experiment	1979	Southern plains USA
26	TIP	Tornado Intercept Project	1975-	USA

The Bow Echo and Mesoscale Convective Vortex Experiment (BAMEX) was conducted over mid-America (Illinois, St. Louis, Missouri) between 20 May and 6 July 2003 (Davies et al., 2004). BAMEX concentrated on studying the life cycle of mesoscale convective systems (MCSs), particularly those producing severe surface winds (bow echoes) and those producing long-lived mesoscale convective vortices (MCVs) capable of initiating subsequent convection. BAMEX investigated competing hypothesis explaining the development of severe straight-line winds. The hypotheses are that they are caused by the production of negative buoyancy in the rear-inflow jet which is a function of the microphysical composition of the stratiform region, that they result from meso gamma scale vortices near the surface along the leading edge of the bow echo, and that they are produced by internal gravity waves produced from perturbations of the stable boundary layer by deep convection. BAMEX also investigated the process of MCV formation which had hitherto not been well observed, and sought to understand how convection is initiated and organized in the vicinity of long-lived MCVs.

The Thunderstorm Electrification and Lightning Experiment (TELEX) was conducted in May–June 2003 and 2004 in central Oklahoma (MacGorman et al., 2008). The objective of the experiment was to study how lightning and other electrical storm properties depend on storm structure, updrafts, and precipitation formation. Measurements were taken by a lightning mapping array, polarimetric and mobile Doppler radars, and balloon-borne electric-field meters and radiosondes. The results showed that the interaction between cloud ice and riming graupel is an essential ingredient in electrifying storms, though it may not account for every region of storm charge.

## 7. Storm Chasing

Storm chasing is the pursuit of any severe weather condition, which can be for curiosity, adventure, scientific investigation, or for news or media coverage. While witnessing a tornado is generally the biggest objective for most chasers, many chase thunderstorms and delight in viewing cumulonimbus and related cloud structures, watching a barrage

of hail and lightning. There are also a smaller number of storm chasers who intercept tropical cyclones and waterspouts. The storm chasing can have scientific objectives by collaborating with an university or government project. A few operate "chase tour" services, making storm chasing a niche for tourism. The first recognized storm chaser is David Hoadley ([https://en.wikipedia.org/wiki/Storm\\_chasing](https://en.wikipedia.org/wiki/Storm_chasing)) who is considered the pioneer storm chaser. He began chasing North Dakota storms in 1956, using data from area weather offices and airports. The most popular stormchasing-tour company was founded by Dr. Reed Timmer of the TV show "Storm Chasers". They specialized in tornado chasing led by an Oklahoma University Meteorologist. Local National Weather Service offices hold storm spotter training classes. Some offices collaborate to produce severe weather workshops oriented toward operational meteorologists. Storm chasers vary with regards to the amount of equipment used, some prefer a minimalist approach; where only basic photographic equipment is taken on a chase, while others use everything from satellite-based tracking systems and live data feeds to vehicle-mounted weather stations and hail guards.

The equipment used for storm chasing are generally (1) Video camera, (2) Digital still camera, (3) Radios (walkie-talkies), (4) smart phones, tablets (5) laptops, loaded with softwares like Weather Display, wind data logger, mobile weather Net, (6) Cabled Weather Station, (7) Doppler On Wheels (DOW), (8) Satellite Weather Receiver, (9) chaser vehicle (10) food and drink. A few storm chaser crews deploy their own Radiosondes. Details may be obtained from some of the storm chaser groups (<http://science.howstuffworks.com/nature/climate-weather/storms/storm-chaser3.htm>; <http://www.rammount.com/blog/2016/04/storm-chasing-tool-kit-an-evolution-in-a-must-have-tech/>; <http://n2kn1.com/storm-chase-equipment/>).

## 8. Summary

Thunderstorms form almost everywhere on the earth. The basic ingredients for their formation are moisture, instability, and lifting. Most of the damages from thunderstorms occur due to



strong winds, lightning strike, hail stones, and flash floods. Numerical models of the storms range from Single Column model to one, two or three dimensional. The forecasting/nowcasting of thunderstorms are done based on the combination of synoptic methods, Doppler Radars, and numerical ensemble models with rapid update cycle data assimilation. The skill of forecasting the thunderstorms have spatial errors of about 40 km, temporal errors  $\pm 30$  minutes and intensity errors about -25 % (underestimated) in 24 hours.

Field experiments are conducted to improve our understanding of the structures, life cycles and develop better models for forecasting the thunderstorms. Many field campaigns are conducted in India since 1929, but a majority of them are conducted in USA in recent years to understand their mechanisms and improve forecasting skills. Storm Chasing has become an adventure, curiosity and hobby in addition to achieving scientific goals. While field campaigns on thunderstorms were conducted in India much before it started in USA, there is a need for more concerted efforts on collecting field observations of severe storms using latest equipments with focused scientific objectives, convective scale data assimilation and ensemble forecasting of the origin, track, lightning strike probability and intensity of the storm fury.

## References

- Albrecht, R., S. Goodman, D. E. Buechler, and T. Chronis, 2009: Tropical frequency and distribution of lightning based on 10 years of observations from space by the lightning imaging sensor (LIS). 4th Conf. Meteorological Applications of Lightning Data, 89th AMS Annual Meeting, 10-15 Jan 2009, Phoenix Arizona, USA.
- Anthes, Richard A. 1990: Recent Applications of the Penn State/NCAR Mesoscale Model to Synoptic, Mesoscale, and Climate Studies. *Bulletin of the American Meteorological Society*: Vol. 71, No. 11, pp. 1610–1629.
- Arakawa, A. and W.H. Schubert, 1974: Interaction of cumulus cloud ensemble with the largescale environment, Part I. *J. Atmos. Sci.*, 31, 674-701.
- Benjamin, S., S. Weygandt, M. Hu, C. Alexander, T. Smirnova, J. Olson, J. Brown, E. James, D. Dowell, G. Grell, H. Lin, S. Peckham, T. Smith, W. Moninger, and G. Manikin, 2016: A northamerican hourly assimilation and model forecast cycle: The rapid refresh. *Mon. Wea. Rev.*, 144, 1669-1694. <https://doi.org/10.1175/MWR-D-15-0242.1>
- Bluestein, H. B., and M. H. Jain, 1985: Formation of mesoscale lines of precipitation: Severe squall lines in Oklahoma during the spring. *J. Atmos. Sci.*, 42, 1711–1732.
- Bright, D. R., J. Huhn, S. J. Weiss, J. J. Levit, J. S. Kain, R. S. Schneider, M. C. Coniglio, M. Duquette, and M. Xue, 2009: Short-range and storm-scale ensemble forecast guidance and its potential applications in air traffic decision support. Preprint, Aviation, Range, Aerospace Meteorology Special Symposium Weather-Air Traffic Management Integration, Phoenix, AZ., Amer. Meteor. Soc., Paper P1.7.
- Bright, D.R. and J.S. Grams, 2009: Short range ensemble forecast (SREF) calibrated thunderstorm probability forecasts: 2007-2008 verification and recent enhancements. Preprints, *3rd Conf. on Meteorological Applications of Lightning Data*, Phoenix, AZ, Amer. Meteor. Soc., 6.3.
- Bright, D.R., M.S. Wandishin, R.E. Jewell, and S.J. Weiss, 2005: A physically based parameter for lightning prediction and its calibration in ensemble forecasts. Preprints, *Conf. on Meteorological Applications of Lightning Data*, San Diego, CA, Amer. Meteor. Soc., CD-ROM, 4.3.
- Case, Jonathan L., Manobianco, John, Oram, Timothy D., Garner, Tim, Blottman, Peter F., Spratt, Scott M. 2002: Local Data Integration over East-Central Florida Using the ARPS Data Analysis System. *Weather and Forecasting*: Vol. 17, No. 1, pp. 3–26.
- Casati, B., Wilson, L. J., Stephenson, D. B., Nurmi, P., Ghelli, A., Pocerich, M., Damtrath, U., Ebert, E. E., Brown, B. G. and Mason, S. (2008) Review, Forecast verification: current status and future directions. *Meteorol. Applications* 15: 3- 18

Casati, B., G. Ross, and D. B. Stephenson, (2004) A new intensity-scale approach for the verification of spatial precipitation forecasts. *Meteor. Appl.* 11: 141–154.

*Center for Severe Weather Research (CSWR), 2006. "Doppler On Wheels". Retrieved 2006-12-29.*

Christian, H. J., and co-authors, 1999: The Lightning Imaging Sensor. *Proc. 11th Int. Conference on Atmospheric Electricity*, Guntersville, AL, International Commission on Atmospheric Electricity, 746-749.

Cotton, William R., Thompson, Gregory, Mieike, Paul W. 1994: Real-Time Mesoscale Prediction on workstations. *Bulletin of the American Meteorological Society*: Vol. 75, No. 3, pp. 349–362.

Cotton, W. R., G. Tripoli, R. Rauber and E. Mulvihill, 1986: Numerical simulation of the effects of varying ice crystal nucleation rates and aggregation processes on orographic snowfall. *J. Appl. Meteor.*, 25, 1658-1680.

Crook, N. A., and J. Sun, 2002: Assimilating radar, surface, and profiler data for the Sydney 2000 forecast demonstration project. *J. Atmos. Oceanic Technol.*, 19, 888–898.

Dalal S, Lohar D, Sarkar S, Sadhukhan I, Debnath GC (2012) Organizational modes of squall-type mesoscale convective systems during premonsoon season over eastern India. *Atmos Res* 106:120–138.

Das Someshwar, A. Sarkar, Mohan K. Das, M. M. Rahman, and M. N. Islam, 2015: Composite Characteristics of Nor'westers based on Observations and Simulations. *Atmospheric Research* (doi: 0.1016/j.atmosres.2015.02.009).

Das Someshwar, U. C. Mohanty, AjitTyagi, D. R. Sikka, P. V. Joseph, L. S. Rathore, A. Habib, S. Baidya, K. Sonam, and A. Sarkar, 2014: The SAARC STORM - A Coordinated Field Experiment on Severe Thunderstorm Observations and Regional Modeling over the South Asian Region. *Bulletin of the American Meteorological Society* (doi: 10.1175/BAMS-D-12-00237.1).

Das Someshwar, 2010: Climatology of thunderstorms over the SAARC region. SMRC

No. 35, Available from SAARC Meteorological Research Centre E-4/C, Agargaon, Dhaka-1207, Bangladesh.

Das Someshwar, B.R.S.B. Basnayake, M.K. Das, M.A.R. Akand, M.M. Rahman, M.A. Sarker and M.N. Islam, 2009: Composite Characteristics of Nor'westers observed by TRMM and Simulated by WRF Model. *SMRC Report No. 25, 44 pp.* (Available from SAARC Meteorological Research centre, E-4/C, Agargaon, Dhaka-1207, Bangladesh).

Das Someshwar, D. Johnson and Wei-Kuo Tao, 1999: Single-Column and Cloud Ensemble Model simulations of TOGA-COARE convective systems. *J. Meteor. Soc. of Japan*, Vol. 77, No. 4, PP 803-826.

Das Someshwar, Y.C. Sud and M.J. Suarez, 1998: Inclusion of a prognostic cloud scheme with the Relaxed Arakawa-Schubert cumulus parameterization; Single Column model studies. *Quart. Jour. of Roy Met. Soc.*, Vol. 124, PP 2671-2692.

Das Someshwar, U.C. Mohanty and O.P. Sharma, 1987: Semiprognostic test of the Arakawa-Schubert cumulus parameterization during different phases of the summer monsoon. *Contrib. Atmos. Phys.*, Vol. 60, No. 2, PP 255-275.

Davis, C., N. Atkins, D. Bartels, L. Bosart, M. Coniglio, G. Bryan, W. Cotton, D. Dowell, B. Jewett, R. Johns, D. Jorgensen, J. Knievel, K. Knupp, W.-C. Lee, G. McFarquhar, J. Moore, R. Pryzbylinski, R. Rauber, B. Smull, J. Trapp, S. Trier, R. Wakimoto, M. Weisman, and C. Ziegler, 2004: The Bow-Echo and MCV Experiment (BAMEX): Observations and opportunities. *Bull. Amer. Meteor. Soc.*, 85, 1075-1093.

Dawn, S. and M. Mandal, 2014: Surface mesoscale features associated with leading convective line-trailing stratiform squall lines over the Gangetic West Bengal. *Meteorology and Atmospheric Physics*, 125 (3-4), 119

Donner, L. J., C. J. Seman, R. S. Hemler, 1999: Three-dimensional cloud-system modeling of GATE Convection. *J. Atmos. Sci.*, 56, 1885–1912.

- Dudhia, J, 1993: A non-hydrostatic version of the Penn State/ NCAR mesoscale model: Validation tests and simulation of an Atlantic cyclone and cold front. *Mon. Wea. Rev.*, 121, 1493-1513.
- Ebert E.E., (2008) Fuzzy verification of high-resolution gridded forecasts: a review and proposed framework. *Meteorol. Appl.*15: 51-64.
- Ebert E.E., McBride J.L., (2000) Verification of precipitation in weather systems: Determination of systematic errors. *Journal of Hydrology*239: 179–202.
- Gilleland E., Ahijevych D., Brown B.G., Casati B., Ebert E.E., (2009) Intercomparison of Spatial Forecast Verification Methods. *Wea. Forecasting*24: 1416-1430.
- Gilmour, I., Smith, L. A. And Buizza, R. 2001: Linear regime duration: Is 24 hours a long time in synoptic weather forecasting? *J. Atmos. Sci.*, 58, 3525–3539
- Grams, J. S., W. A. Gallus Jr., S. E. Koch, L. S. Wharton, A. Loughe, and E. E. Ebert, 2006: The use of a modified Ebert–McBride technique to evaluate mesoscale model QPF as a function of convective system morphology during IHOP 2002. *Wea. Forecasting*, 21, 288–306.
- Houze, R.A., B. F. Smull, and P. Dodge, 1990: Mesoscale organization of springtime rainstorms in Oklahoma. *Mon. Wea. Rev.*, 118, 613–654.
- Hsu S.A. and Zhongde Yana, 1998: A Note on the Radius of Maximum Winds for Hurricanes. *Journal of Coastal Research*. Coastal Education & Research Foundation, Inc. 12 (2): 667–668.
- IMD, 1944: Nor'wester of Bengal. India Meteorological Department Tech. Note 10. 17 pp.
- Johnson, D. E., P. K. Wang, and J. M. Straka, 1993: Numerical simulation of the 2 August 1981 CCOPE supercell storm with and without ice microphysics. *J.Appl. Meteor.*, **32**, 745-759.
- JMA, 2017*: "Western North Pacific Typhoon best track file 1951–2017". *Japan Meteorological Agency. 2010-01-13. Retrieved 2010-01-13.*
- Jung, J.-H., and A. Arakawa, 2007: A three-dimensional cloud model based on the vector vorticity equation. Colorado State University Atmospheric Science Paper 762, 57 pp. [Available online at [http://kiwi.atmos.colostate.edu/pubs/joon-heetech\\_report.pdf](http://kiwi.atmos.colostate.edu/pubs/joon-heetech_report.pdf).]
- Jung, J.-H., and A. Arakawa, 2008: A three-dimensional anelastic model based on the vorticity equation. *Mon. Wea. Rev.*, vol., 136, 276-294.
- Karmakar, S., and M.M. Alam, 2007: Tropospheric moisture and its relationship with rainfall due to norwesters in Bangladesh. *Mausam* 58: 153-160.
- Karmakar, S., and M.M. Alam, 2006: Instability of the troposphere associated with thunderstorms/ norwesters over Bangladesh during the pre-monsoon season. *Mausam* 57, 629-638.
- Karmakar, S., and M.M. Alam, 2005: On the sensible heat energy, latent heat energy and potential energy of the troposphere over Dhaka before the occurrence of Nor'westers in Bangladesh during the pre-monsoon season. *Mausam*, 56: 671-680.
- Karmakar, S., 2001: Climatology of thunderstorm days over Bangladesh during the pre- monsoon season. *Bangladesh J. Sci. and Tech.*, 3 (1): 103-112.
- Litta A. J, U. C. Mohanty, S. Dasand S. M. Ididcula, (2012) Numerical Simulation of Severe Local Storms over East India using WRF-NMM mesoscale model. *Jour. Atmos. Res.*  
<http://dx.doi.org/10.1016/j.atmosres.2012.04.015>
- Lin, Y.-L., R.D. Farley, and H.D. Orville, 1983: Bulk parameterization of the snow field in a cloud model. *J. Climate Appl. Meteor.*, 22, 1065– 1092.
- Liu, Changhai, Moncrieff, Mitchell W., Grabowski, Wojciech W. 2001: Explicit and Parameterized Realizations of Convective Cloud Systems in TOGA COARE.*Monthly*

- Weather Review*: Vol. 129, No. 7, pp. 1689–1703.
- MacGorman, D. R., W. D. Rust, T. J. Schuur, M. I. Biggerstaff, J. M. Straka, C. L. Ziegler, E. R. Mansell, E. C. Bruning, K. M. Kuhlman, N. R. Lund, N. S. Biermann, C. Payne, L. D. Carey, P. R. Krehbiel, W. Rison, K. B. Eack, and W. H. Beasley, 2008: TELEX: The thunderstorm electrification and lightning experiment. *Bull. Amer. Meteor. Soc.*, 89, 997–1018.
- McCumber, M., W. K. Tao, J. Simpson, R. Penc, and S. T. Soong, 1991: Comparison of ice-phase microphysical parameterization schemes using numerical simulations of tropical convection. *J. Appl. Meteor.*, 30, 985–1004.
- Mesinger, Fedor. 1996: Improvements in Quantitative Precipitation Forecasts with the Eta Regional Model at the National Centers for Environmental Prediction: The 48-km Upgrade. *Bulletin of the American Meteorological Society*: Vol. 77, No. 11, pp. 2637–2650.
- Mohanty, U. C., and Coauthors, 2006: Weather summary during pilot experiment of Severe Thunderstorms Observations and Regional Modeling (STORM) programme. India Department of Science and Technology Rep., 177 pp.
- Mohanty, U.C. and Coauthors, 2007: Weather summary during pilot experiment of Severe Thunderstorms Observations and Regional Modeling (STORM) programme. India Department of Science and Technology Rep., 179 pp.
- National Hurricane Center; (NHC), 2016. "The Northeast and North Central Pacific hurricane database 1949–2016". United States National Oceanic and Atmospheric Administration's National Weather Service.
- Nitta, T., 1975: Observational determination of cloud mass flux distribution. *J. Atmos. Sci.*, 32, 73–91.
- Ogura, Y., and N. A. Phillips, 1962: Scale analysis of deep and shallow convection in the atmosphere. *J. Atmos. Sci.*, 19, 173–179.
- Parker, M. D., and R. H. Johnson, 2000: Organizational modes of midlatitudemesoscale convective systems. *Mon. Wea. Rev.*, 128, 3413–3436.
- Rasmussen, E. N., J. M. Straka, R. P. Davies-Jones, C. A. Doswell, F. H. Carr, M. D. Eilts, and D. R. MacGorman, 1994: Verification of the Origins of Rotation in Tornadoes Experiment: VORTEX. *Bull. Amer. Meteor. Soc.*, 75, 995–1006.
- Roberts N.M., Lean H.W., (2008) Scale-selective verification of rainfall accumulations from high resolution forecast of convective events. *Mon. Wea. Rev.* 136: 78–97.
- Roy Bhowmik, S. K., Sen Roy, S., Srivastava, K., Mukhopadhyay, B., Thamp, S.B., Reddy Y. K., Singh, H, Venkateswarlu, S., Adhikary, S (2011) Processing of Indian Doppler Weather Radar data for mesoscale applications, *MeteorolAtmosPhys*, 2011: 133-147
- Sarkar Abhijit, Someshwar Das, and Devajyoti Dutta, 2016: A New Approach to Determine skills of NWP Model in Forecasting Thunderstorms Based on Doppler Weather Radar Observations. *Submitted to Atmosfera*.
- Soong, S.-T., and W.-K. Tao, 1980: Response of deep tropical clouds to mesoscale processes. *J. Atmos. Sci.*, 37, 2016–2036.
- Srivastava, K., Gao, J., Brewster, K., Roy Bhowmik, S. K., Xue, M., Gadi, R., (2011) Assimilation of Indian radar data with ADAS and 3DVAR techniques for simulation of a small-scale tropical cyclone using ARPS model, *Nat Hazards*, DOI 10.1007/s11069-010-9640-4.
- STORM, 2005: STORM science plan. India Department of Science and Technology Rep., 118 pp. [Available online at [www.imd.gov.in/SciencePlanofFDPs/STORM%20Science%20Plan.pdf](http://www.imd.gov.in/SciencePlanofFDPs/STORM%20Science%20Plan.pdf).]
- Sun, J., M. Chen, and Y. Wang, 2010: A frequent-updating analysis system based on radar, surface, and mesoscale model data for the Beijing 2008 Forecast Demonstration Project. *Wea. Forecasting*, 25, 1715–1735.
- Sun, J., 2005: Convective-scale assimilation of radar data: Progress and challenges. *Quart. J. Roy. Meteor. Soc.*, 131, 3439–3463.

- Sun, J. and Crook, N. A. 1998: Dynamical and microphysical retrieval from Doppler radar observations using a cloud model and its adjoint: II. Retrieval experiments of an observed Florida convective storm. *J. Atmos. Sci.*, **55**, 835–852
- Sun, J. and Crook, N. A. 1997: Dynamical and microphysical retrieval from Doppler radar observations using a cloud model and its adjoint: I. model development and simulated data experiments. *J. Atmos. Sci.*, **54**, 1642–1661
- Tao, W.-K., and S.-T. Soong, 1986: A study of the response of deep tropical clouds to mesoscale processes: Three-dimensional numerical experiments. *J. Atmos. Sci.*, **43**, 2653-2676.
- Tao, Wei-kuo, Simpson, Joanne, Soong, Su-Tzai. 1987: Statistical Properties of a Cloud Ensemble: A Numerical Study. *Journal of the Atmospheric Sciences*: Vol. 44, No. 21, pp. 3175–3187.
- Toth, Zoltan. 2001: meeting summary: Ensemble Forecasting in WRF. *Bulletin of the American Meteorological Society*: Vol. 82, No. 4, pp. 695–698.
- Tyagi A., D.R. Sikka, Suman Goyal and Mansi Bhowmick, 2012: A satellite based study of pre-monsoon thunderstorms (Nor'westers) over eastern India and their organization into mesoscale convective complexes. *Mausam*, **63**, 1, 29-54
- Tyagi, A., 2007: Thunderstorm climatology over Indian region. *Mausam* **58**: 189–212
- United States Department of Energy (USDE), 2009: "Natural Phenomena Hazards Design and Evaluation Criteria for Department of Energy: E.2.2 Additional Adverse Effects of Tornadoes". p. E7. Retrieved 2009-11-20.
- Walter A. Lyons, 1997: *The Handy Weather Answer Book*. Detroit: Visible Ink Press.
- Wurman J., David Dowell, Yvette Richardson, Paul Markowski, Erik Rasmussen, Donald Burgess, Louis Wicker, and Howard B. Bluestein, 2012: The Second Verification of the Origins of Rotation in Tornadoes Experiment: VORTEX2. *Bull. Amer. Meteor. Soc.*, **93**, 1147–1170.
- Wurman, Joshua; C. Alexander; P. Robinson; Y. Richardson, 2007: "Low-Level Winds in Tornadoes and Potential Catastrophic Tornado Impacts in Urban Areas". *Bulletin of the American Meteorological Society*. American Meteorological Society. **88** (1): 31–46.
- Xu, Kuan-Man, Randall, David A. 1996: Explicit Simulation of Cumulus Ensembles with the GATE Phase III Data: Comparison with Observations. *Journal of the Atmospheric Sciences*: Vol. 53, No. 24, pp. 3710–3736.
- Yamane, Y., T. Hayashi, A. M. Dewan, and Fatima Akter, 2009a: Severe local convective storms in Bangladesh: Part I. Climatology. *Atmos. Research*, **95**, 4, 400–406. DOI: 10.1016/j.atmosres.2009.11.004.
- Yamane, Y., T. Hayashi, A. M. Dewan, and Fatima Akter, 2009b: Severe local convective storms in Bangladesh: Part II. Environmental Conditions. *Atmos Research*, **95**, 4: 407- 418. DOI: 10.1016/j.atmosres.2009.11.003.
- Yamane, Y., and Hayashi, T., 2006: Evaluation of environmental conditions for the formation of severe local storms across the Indian subcontinent. *Geophys. Res. Lett.* **33**, L17806. doi:10.1029/2006GL026823.
- Yanai, M., Esbensen, S. and Chu, J., 1973: Determination of bulk properties of tropical cloud clusters from large scale heat and moisture budgets. *J. Atmos. Sci.*, **30**, 611-627.